remote sensing

Article

Evaluation of MERRA-2 Aerosol Optical and Component Properties over China Using SONET and PARASOL/GRASP Data

Yang Ou [1,2,†], Zhengqiang Li [1,2,*], Cheng Chen [3,†], Ying Zhang [1,2], Kaitao Li [1], Zheng Shi [1,2], Jiantao Dong [1], Hua Xu [1,2], Zongren Peng [1], Yisong Xie [1] and Jie Luo [1]

[1] State Environmental Protection Key Laboratory of Satellite Remote Sensing, Aerospace Information Research Institute, Chinese Academy of Sciences, Beijing 100101, China; ouyang2018@radi.ac.cn (Y.O.); zhangying02@radi.ac.cn (Y.Z.); likt@radi.ac.cn (K.L.); shizheng@radi.ac.cn (Z.S.); 2016043020@cuit.edu.cn (J.D.); xuhua@radi.ac.cn (H.X.); pengzr@aircas.ac.cn (Z.P.); xieys@radi.ac.cn (Y.X.); luojie@aircas.ac.cn (J.L.)
[2] University of Chinese Academy of Sciences, Beijing 100049, China
[3] GRASP-SAS, Remote Sensing Developments, Cite Scientifique, University Lille, 59655 Villeneuve d'Ascq, France; cheng.chen@grasp-sas.com
* Correspondence: lizq@radi.ac.cn
† These authors contributed equally to this work.

Abstract: The Modern-Era Retrospective analysis for Research and Applications, Version 2 (MERRA-2) is widely used as an advanced model dataset for the understanding of global climate change. However, independent validation and comparison of MERRA-2 are both insufficient and always desired. Therefore, in this study, the quantitative evaluation of MERRA-2 aerosol products was conducted over China for Aerosol Optical Depth (AOD), Angstrom exponent (AE), absorbing AOD (AAOD) and chemical components (black carbon (BC) and dust (DU)) using Sun sky radiometer Observation NETwork (SONET) ground-based measurements and POLDER-3/PARASOL satellite products generated by the GRASP algorithm. The available MERRA-2 monthly dataset and PARASOL/GRASP monthly and seasonal products were intercompared over China. MERRA-2 AOD (550 nm) show general good agreement with SONET and PARASOL/GRASP. For example, the correlation coefficients are usually 0.6–0.85 with SONET and 0.75–0.85 with PARASOL/GRASP, the bias is usually −0.293 to +0.008 with SONET. For AE and AAOD, the agreement is still reasonable. MERRA-2 is found to overestimate fine mode AE and to display a general underestimation of aerosol absorption over China. In addition, MERRA-2 BC and DU mass concentrations show spatial and quantitative consistency with PARASOL/GRASP components climatological products. The relatively high columnar BC mass concentration is observed around 1.5–2 mg/m^3 over the East China industrial region and high DU mass concentration is around 150 mg/m^3 near Taklimakan desert. MERRA-2 shows slightly higher BC and lower DU concentration than PARASOL/GRASP over East China. The evaluations with in situ BC measurements near surface verify the overestimation (MAE = +0.44 μg/m^2) of MERRA-2 and underestimation (MAE = −0.38 μg/m^2) of PARASOL/GRASP. The analysis demonstrates multi-source datasets, such as ground-based, space-borne remote sensing, in situ measurements, model simulation as well as reanalysis data, complement each other and can be used to refine aerosol characterization.

Keywords: MERRA-2; SONET; PARASOL/GRASP; aerosol components; aerosol optical properties

check for updates

Citation: Ou, Y.; Li, Z.; Chen, C.; Zhang, Y.; Li, K.; Shi, Z.; Dong, J.; Xu, H.; Peng, Z.; Xie, Y.; et al. Evaluation of MERRA-2 Aerosol Optical and Component Properties over China Using SONET and PARASOL/GRASP Data. *Remote Sens.* **2022**, *14*, 821. https://doi.org/10.3390/rs14040821

Academic Editor: Carmine Serio

Received: 27 December 2021
Accepted: 7 February 2022
Published: 9 February 2022

1. Introduction

Atmospheric aerosol refers to a relatively stable suspension system in which liquid or solid particles are uniformly dispersed in the gas and it is an important substance in the atmosphere [1]. Aerosol components can be categorized by its sources, such as desert dust, sea spay, biomass burning, black carbon, organic matter, sulfates, etc. [2]. Although its content is very small in the atmosphere, atmospheric aerosol plays a significant role in the radiation balance of the Earth's atmosphere system and it affects precipitation [3]. In addition, black carbon aerosol emitted from biomass burning is a strong carcinogen and can lead to cardiovascular and cerebrovascular diseases [4].

In recent years, many researchers have performed various studies on atmospheric aerosol's optical and microphysical properties as well as their chemical components [5–7]. A series of ground-based, space-borne and model-simulated aerosol data is generated for the community. The National Aeronautics and Space Administration (NASA) released the global reanalysis dataset Modern-Era Retrospective analysis for Research and Applications, Version 2 (MERRA-2) in 2016 [7]. MERRA-2 aerosol dataset is of a spatial resolution of 0.625° (longitude) × 0.5° (latitude) and a temporal resolution of up to an hour. MERRA-2 also contains vertical resolved aerosol optical and composition information, and the product provides the characteristics with the advantages of continuous time and comprehensive spatial coverage. It is widely used in a series of scientific research, such as climate assessment [8–10]. However, aerosol compositions are complex and very uncertain due to the high variability in their temporal and spatial distribution [11]. A series of previous studies have reported the validation of the MERRA-2 dataset, but the selection of the validation dataset is unsuitable [12–14]. For instance, previous studies have compared the MERRA-2 Aerosol Optical Depth (AOD) with ground-based observations from Aerosol Robotic NETwork (AERONET) in China, which proved that the data of MERRA-2 and AERONET sites are consistent in China [12,13]. Previous results also described the comparison of the spatial distribution of AOD product from MERRA-2 with AOD from Moderate-resolution Imaging Spectroradiometer (MODIS) [8,10,12,15]. It was found that MERRA-2 can capture the temporal and spatial sequentially changes in AOD very well except for heavy pollution conditions [12]. There is a clear underestimation of high aerosol loading phenomenon that is similar to MODIS. Using MERRA-2 AOD products to carry out a long-term series study on China's economically developed regions shows that AOD has had a continuously increasing trend of fluctuations in recent years [16]. In fact, these validations are within the expectation, since MERRA-2 has already assimilated the AOD from AERONET and MODIS [17,18]. Therefore, it is necessary to use other independent ground-based data and satellite products than the third-party remote sensing dataset to further verify and evaluate MERRA-2 products. Obviously, it is crucial to estimate aerosol's optical and chemical parameters by independent data.

Generalized Retrieval of Aerosol and Surface Properties (GRASP) is a highly accurate aerosol retrieval algorithm that derives the properties of aerosol and surface simultaneously [19–21]. It is a statistically optimized fitting of the observations using the multi-term least square method. It has been applied on POLDER multiangle polarization satellite and provided a series of aerosol products for POLDER (see the details in the paper by [22]) which mainly included AOD, Angstrom exponent (AE), absorbing aerosol optical depth (AAOD), etc. These parameters can reflect the aerosol content and size information in the columnar atmosphere. As previously described, Wei et al. [23] used ground-based observation data from Sun sky radiometer Observation NETwork (SONET) to verify GRASP products over China, and the results showed that GRASP products are of good accuracy [23].

Sun sky radiometer Observation NETwork (SONET) is a ground-based aerosol automatic monitoring and observation network established throughout China by the Aerospace Information Research Institute the Chinese Academy of Sciences in 2009 [24]. SONET has undergone strict calibration procedure every year and has a similar accuracy as AERONET [25,26]. It is widely used in the validation of satellite retrieval results and the establishment of aerosol models with high reliability [23,27].

Consequently, this study uses ground-based SONET data and satellite GRASP products to systematically evaluate the applicability of MERRA-2 products in China. It is helpful to improve the numerical simulation of aerosols and towards refine the aerosol effects on climate change.

2. Data and Method

2.1. MERRA-2

The MERRA-2 assimilation system is based on the fifth-generation Goddard Earth Observing System Model, Version 5 (GEOS-5) [15]. This model is coupled with the GOCART chemistry module which simulates five types of aerosols (black carbon, sand dust, organic carbon, sulfate, and sea salt) [28]. For aerosol dataset, MEERA-2 assimilate aerosol data from ground-based AERONET a and space-borne aerosol products from Advanced Very High-Resolution Radiometer (AVHRR), Multi-angle Imaging Spectro Radiometer (MISR) and MODIS [17,18]. MERRA-2 aerosol dataset includes the five types of aerosols' optical properties, emissions, deposition, and aerosol mixing ratios, vertically. For example, aerosol optical property products include aerosol extinction optical thickness at 550 nm, aerosol scattering optical thickness at 550 nm and aerosol angstrom exponent (470–870 nm) for total as well as five aerosol components. The temporal and spatial resolution of the data is 0.625 degrees $\times$ 0.5 degrees, and there are three temporal resolutions: monthly, hourly and every three hours. In the vertical direction, MERRA-2 aerosol dataset is divided into 72 layers from surface to 0.01 hPa. MERRA-2's data cover the period from 1980 to the present, and they include 21 types of products, such as atmospheric aerosols, radiation, temperature, water vapor, precipitation etc. In this study, we use the hourly aerosol component column concentration data product (MERRA-2-2D-tavg-aer***), monthly average aerosol component column concentration data product (MERRA-2_400.inst3_3d_aer***) and surface aerosol component mass concentration product (MERRA-2_400.inst3_3d_aer***). Hourly aerosol optical and component products are firstly validated with ground-based observations (SONET and in situ measurements). Then the monthly products are evaluated with satellite dataset from POLDER-3/GRASP.

2.2. SONET

SONET is a ground-based Cimel radiometer aerosol observation network with a multiwavelength polarization measurement over China, which was established by the Chinese Academy of Sciences [24]. CE-318 solar photometers are used to measure direct-sun and sky radiances, and long-term columnar aerosol optical property, microphysical and radiation characteristic data are then derived and released at http://www.sonet.ac.cn/ (accessed on 1 January 2022). The solar sky photometer CE318 is manufactured by the French company CIMEL Electronique that measures direct sun at eight spectral bands (340, 380, 440, 500, 675, 870, 1020, 1640 nm). The instrument has a full-angle field of view of approximately 1.2°. The CE318 detector measures the spectral extinction of direct beam radiation observations at all 8 bands. Then, based on multispectral and multiangle measurements, the polynomial least-squares method is used to invert the optical and microphysical properties of aerosols. Automatic cloud screens, pre-calibration and post-calibration coefficient interpolation, and expert checks were applied on the screening to generate level 2.0 product. In general, SONET dataset has the approved reliability that is often used as "ground true value" for validation of satellite remote sensing and model simulation results [23,29,30]. The general range of AOD error is about 0.002 [24]. In this study, SONET level-2 products were used to ensure data quality. The 12 SONET automated sites (as shown in Figure 1) are located in typical areas of China. Instrument calibration was performed once a year for each site to ensure data quality [25,26]. Table 1 lists the basic information of the 12 sites classified by four typical climate zones. They are located in typical regions of China, including urban, dust, maritime, and maritime and urban.

In addition, we verify the MERRA-2 black carbon mass concentration with the synchronous in situ measurement using the handheld black carbon meter (Aethalometer) AE-51. The synchronous observation experiment at Beijing site uses a handheld black carbon detector produced by Magee Scientific, and the model is MicroAeth Model AE-51 (AE-51). The instrument uses the principle of optical absorption to collect and analyze the mass concentration of black carbon aerosol in real time. It has the advantages of real-time, high efficiency, and stability. The instrument collects particles in the air onto the quartz filter membrane. The light with a known source intensity is used to measure the attenuation of light scattered by aerosol particles. This part of the attenuation is believed to be caused by black carbon absorption. Therefore, real-time measurement of the mass concentration of black carbon can be achieved through continuous measurement.

Table 1. Basic information on the 12 SONET sites.

Sites.	Longitude/ Latitude	Altitude(m)	Time (Start Time)	Aerosol Characteristics
Beijing	116.4 E, 40.0 N	59	2010.03-	Urban
Guangzhou	113.4 E, 23.1 N	28	2011.11-	Maritime and urban
Zhangye	100.4 E, 38.9 N	1364	2012.07-	Dust
Harbin	126.6 E, 45.7 N	223	2013.12-	Urban
Hefei	117.2 E, 31.9 N	36	2013.01-	Urban
Minqin	103.1 E, 38.6 N	1589	2012.02-	Dust
Nanjing	119.0 E, 32.1 N	52	2013.01-	Urban
Shanghai	121.4 E, 31.3 N	84	2013.03-	Maritime and urban
Xi'an	109.0 E, 34.2 N	389	2012.05-	Urban
Zhoushan	122.2 E, 30.0 N	29	2012.01-	Maritime
Chengdu	104.0 E, 30.6 N	510	2013.05-	Urban
Songshan	113.1 E, 34.5 N	475	2013.11-	Urban

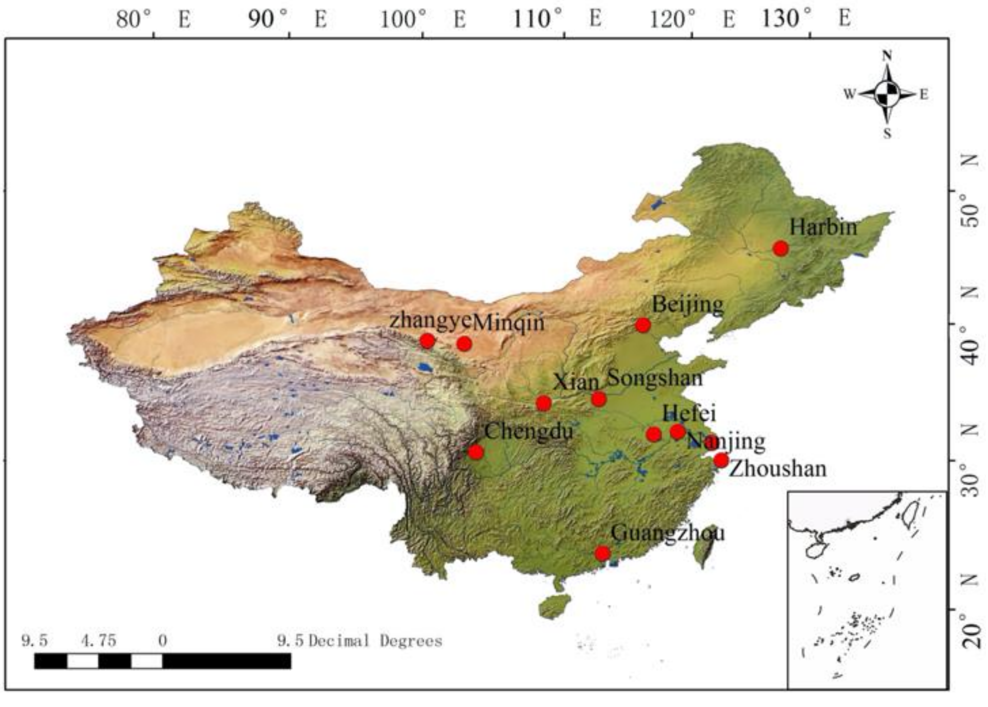

Figure 1. Map of 12 SONET sites in China.

2.3. PARASOL/GRASP

GRASP is a highly rigorous and versatile aerosol and surface retrieval algorithm [19–21], and it is open source at https://www.grasp-open.com (accessed on 1 January 2022). Benefit from the modularization of aerosol/surface modeling and inversion, the algorithm can be applied (with minimal changes) to invert observations from different satellite sensors and ground-based instruments [29,31–34]. A full description of the main "Forward Model" and "Numerical Retrieval" algorithm modules is provided by Dubovik et al. [19]. It provides the retrieved aerosol properties, such as aerosol size distribution, complex index of refraction for fine and coarse mode, single scattering albedo, ratio of spherical particles, height, chemical components of aerosol, and the spectral parameters of surface Bidirectional Reflectance Distribution Function (BRDF) and Bidirectional Polarization Distribution Function (BPDF), simultaneously. GRASP algorithm has been applied on the POLDER series multiangular polarization measurements and generated a series of products by assumption of different aerosol models [22]. Specifically, there are four products of PARASOL/GRASP datasets: «optimized» were optimized to achieve the best tread-off between speed of processing and accuracy of results by radiative transfer calculations; «high-precision» used the accurate radiative transfer calculations; «models» assumed aerosol as external mixture of several aerosol components to be calculated; «components» used an internal mixture retrieved parameters including aerosol size distribution together with volume fractions of the assumed components. The products have been comprehensively evaluated [23]. Chen et al. [22] and Wei et al. [23] have validated and discussed the AOD accuracy of the PARASOL/GRASP products and intercompared with MODIS products. Based on the validation with ground-based measurements (AERONET and SONET), both MODIS and PARASOL AOD products show high accuracy; for example, over land there are 45–55% of the pixels satisfying Global Climate Observing System (GCOS) requirements, max (0.04, 10% AOD), and over ocean the GCOS fractions are usually higher than 55% for both products. In addition, the biases over land and ocean are within 0.03.

GRASP/Component assumes internal mixture based on Maxwell–Garnett effective medium approximation [29]. The PARASOL GRASP/Component product validation by Zhang et al. [35] showed the reliability and comparable accuracy of aerosol optical properties such as AOD, AE, SSA, with the other PARASOL/GRASP products. On the other hand, the advantage of GRASP/Component product is the capability to derive columnar concentration of aerosol components. The evaluation by Li et al. showed reasonable agreement with in situ measurements, for example, the overall mean absolute error for BC is about 2.7 $\mu g/m^3$ and the relative difference is around 40% with respect to the in situ measurements. As shown in Chen et al. [22], «models» provides very consistent results with «high-precision», while «models» shows good accuracy of AOD, and «high-precision» shows strength to capture more detailed aerosol properties. «components» product is validated by Zhang et al. [35] and the accuracy is in general consistent with the other three products. It can derive additional information of columnar aerosol component concentrations. In this study, the AOD, AE, AAOD are from «models» datasets. The BC and DU columnar concentrations are adopted from «components» datasets. A more detailed description of products generated by the GRASP algorithm can be found at the website of https://www.grasp-open.com/products/ (accessed on 1 January 2022).

2.4. Method

The purpose of this study is to evaluate MERRA-2 aerosol products, including AOD, AE, AAOD, and aerosol composition, over China using independent SONET and PARASOL/GRASP dataset. Thus, we match pixels for SONET sun photometers and MERRA-2 in space and time windows. According to the space and time window by Wei et al. [23], the average value of a 3 × 3 window grid centered on the ground site is used. However, the spatial resolution of MERRA-2 was 0.6 degree. The nearest matching method of pixel center coordinates is used in this study. The average value obtained within 30 min before and after the MERRA-2 time is extracted from the SONET observations to verify the MERRA-2 AOD, AE and AAOD. In order to evaluate PARASOL/GRASP and MERRA-2 AOD, AE and AAOD, we first resample PARASOL/GRASP Level 3 0.1 degree products to the same spatial resolution as MERRA-2 and then compare monthly products between MERRA-2 and GRASP. For the validation of black carbon (BC), we used the hourly average value of BC observed by the black carbon meter (AE-51) to match with the hourly average value of MERRA-2.

Since the SONET measured AOD is the closet at 500 nm and the MERRA-2 AOD is at 550 nm. Hence, the SONET AOD is interpolated to 550 nm using AE (α) [23]:

$$AOD_{550} = AOD_{500} \times (550/500)^{-\alpha}, \tag{1}$$

where AOD_{500} is the AOD at 500 nm, AOD_{550} is the AOD at 550 nm, and α is the wavelength index of 440~870 nm.

The statistical indicators used to evaluate the results of MERRA-2 include the correlation coefficient (r), the slope and offset of the linear fitting line, the mean absolute error (MAE), the root mean square error (RMSE), and the expected error (EE) fraction (good fraction, Gfrac) [23,36]. Gfrac represents the ratio of actual results to expected results. The expected result is a retrieved result with an absolute error less than EE. For instance, for the three different aerosol optical parameters AOD, AE and AAOD, we chose different EEs as the expected result. Equations (2) and (3) define MAE and RMSE, Equations (4)–(6) define AOD_{EE}, AE_{EE}, and $AAOD_{EE}$, respectively. X represents the AOD, AE and AAOD.

$$\mathrm{MAE} = \frac{1}{n}\sum_{i=1}^{n}\left|X_{MERRA-2} - X_{GRASP}\right|, \tag{2}$$

$$\mathrm{RMSE} = \sqrt{\frac{1}{n}\sum_{i=1}^{n}\left(X_{MERRA-2} - X_{GRASP}\right)^2}, \tag{3}$$

$$AOD_{EE} = \pm 0.05 \pm 0.15 \times AOD, \tag{4}$$

$$AE_{EE} = AE \pm 0.3, \tag{5}$$

$$AAOD_{EE} = \pm 0.01 \pm 0.1 \times AAOD, \tag{6}$$

3. Results

3.1. Validation of MEERA-2 AOD with SONET

Figure 2 shows the scatter density validation plots of MERRA-2 and ground-based SONET AOD (550 nm) at 12 sites. The color indicates the number of data points. The correlation coefficient (R), root mean square error (RMSE), bias (bias), and expected error (EE), and the intercept and slope of the fitting equation are used to evaluate the accuracy. The study period is ranging from January 2011 to December 2013. The maximum amount of matching points is observed at Beijing (2010), and the overall validation metrics are with R = 0.735, bias = −0.157, RMSE = 0.312 and within EE = 55.62%. As Table 2, the AOD consistency is the best at Zhoushan (a coastal site), with the maximum R = 0.822, bias = −0.044, RMSE = 0.169 and within EE = 69.87%. The maximum expected error is at Zhangye (a rural site near the Gobi Desert) 80% within EE, but R is only 0.634. The overall error of the Xi'an site is relatively large, with R = 0.676, bias = −0.293, RMSE = 0.366, an EE minimum of 25.77%, and a maximum underestimation fraction of 73.71%. One potential reason is that the general complex topography superposed with strong industrial emissions makes it difficult for the simulation to capture all the features at a relatively coarse spatial resolution [37,38]. Wei et al. [23] validate PARASOL/GRASP AOD with SONET showed that the total AOD at 490 nm obtained by the "models" method is of the best consistency with SONET, and the correlation coefficient is 0.96, RMSE 0.14 and approximately 76% of the retrievals are within the scope of Gfrac.

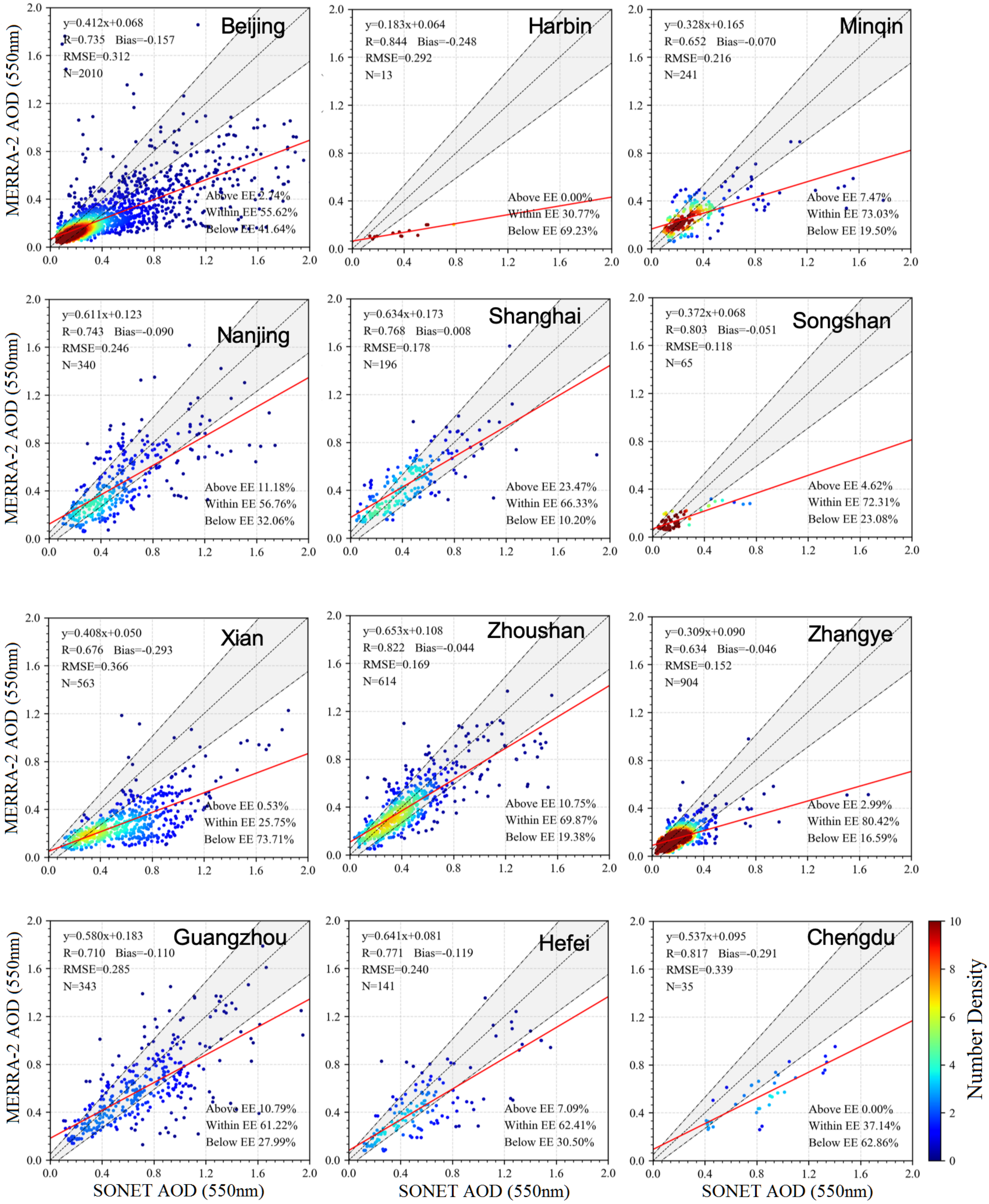

Figure 2. Validation of MERRA-2 AOD (550 nm) with SONET measurements at 12 sites over China. The grey dashed line represents the one-to-one line and EE line. The red solid line represents the linear fitting line.

Figure 3 shows that spatial distribution of AOD difference over 12 sites. The Pearl River Delta (PRD) and the Yangtze River Delta (YRD) sites (Guangzhou, Shanghai, Nanjing, etc.) are mainly affected by the ocean monsoon climate with annual average AOD 0.4–0.5. The Xi'an site has the highest AOD, with an annual mean AOD 0.75 from 2011 to 2013. The Chengdu site is located in the Sichuan Basin, where an annual AOD (0.58) is the second largest. MERRA-2 generally underestimates sites with high AOD, the overall bias is 0.22 for all sites. Moreover, for the Beijing site, MERRA-2 underestimates the AOD value of 0.08 as Figure 3b. The lowest annual mean AOD is 0.19 appeared in the Zhangye rural site. This is related to the small population and the dominant natural dust. MERRA-2 also underestimates these sites with low AOD values, with an underestimation of 0 to 0.04.

As shown in Figure 3d, the probability densities functions (PDFs), the AOD value of the MERRA-2 model is slightly lower than that of the SONET products, mainly concentrated in the range of +/−0.1, and the overall MERRA-2 is lower by 0.145 (Figure 3d). This may be due to the assimilated MODIS TERRA and AQUA AOD, which is proved to be underestimated in many studied over China [39,40].

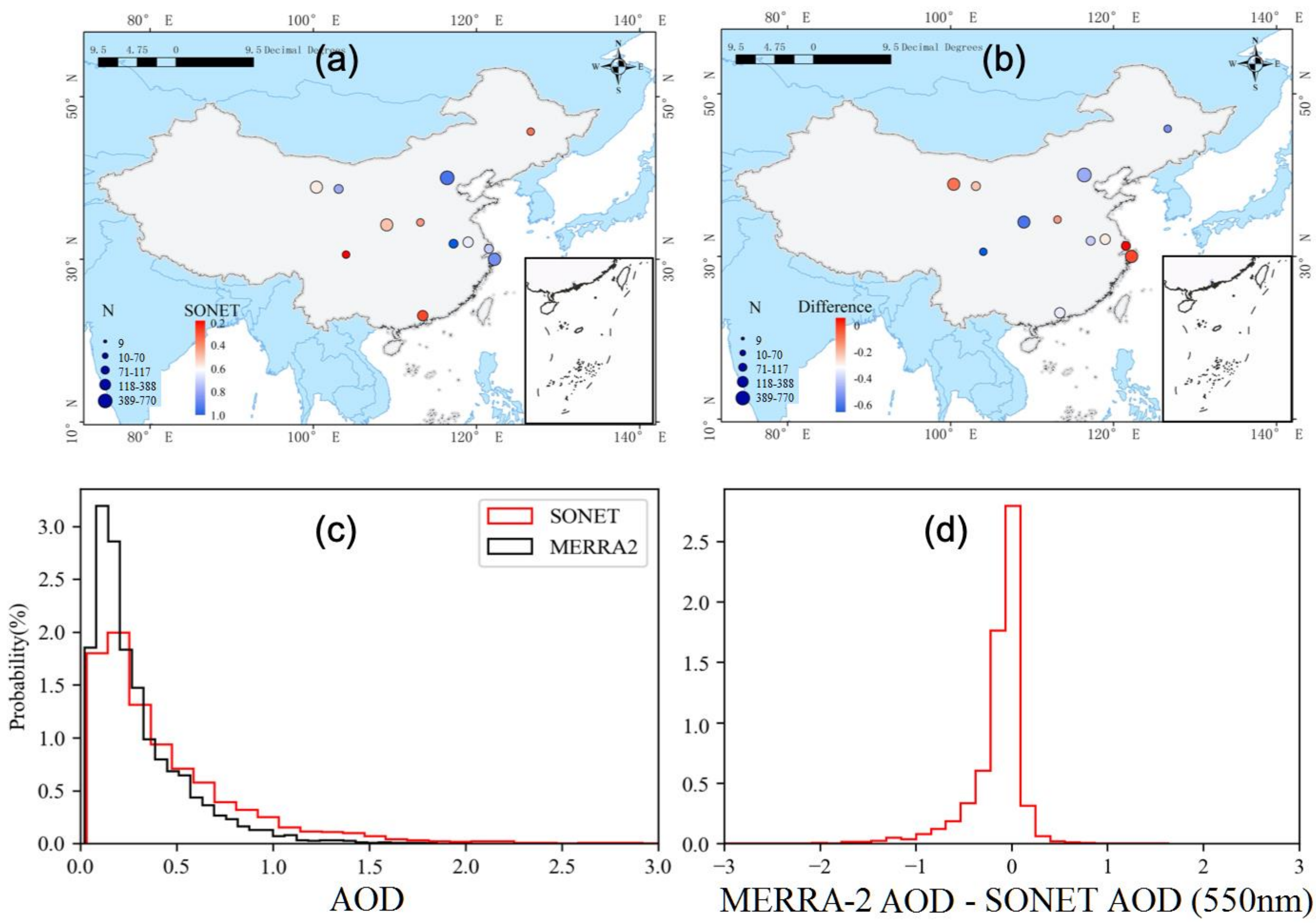

Figure 3. (**a**) The statistics mean of the AOD (550 nm) at 12 SONET sites over China from January 2011 to December 2013. (**b**) The differences of MERRA-2 and SONET AOD (550 nm) from 2011 to 2013. Color represents the values and circle size represents the numbers of matched points. (**c**) The probability density functions (PDFs) of the MERRA-2 and SONET AOD (550 nm). (**d**) PDF for AOD (550 nm) difference ($AOD_{MERRA\text{-}2}$–AOD_{SONET}) between MERRA-2 and SONET.

Table 2. The statistics R, RMSE, bias of AOD, AE, AAOD of the MERRA-2.

	AOD			AE			AAOD		
	R	**RMSE**	**Bias**	**R**	**RMSE**	**Bias**	**R**	**RMSE**	**Bias**
Beijing	0.735	0.312	−0.157	0.506	0.308	0.030	0.546	0.034	−0.018
Harbin	0.844	0.292	−0.248	0.377	0.180	−0.139	−0.453	0.028	−0.018
Minqin	0.652	0.216	−0.070	0.733	0.217	0.005	−0.139	0.032	−0.015
Nanjing	0.743	0.246	−0.090	0.529	0.288	0.160	0.418	0.030	−0.004
Shanghai	0.768	0.178	0.008	0.575	0.265	0.076	0.605	0.022	0.008
Songshan	0.803	0.118	−0.051	0.522	0.313	0.195	0.284	0.019	−0.010
Xi'an	0.676	0.366	−0.293	0.624	0.326	0.001	0.263	0.058	−0.040
Zhoushan	0.822	0.169	−0.044	0.546	0.289	0.063	0.572	0.022	0.012
Zhangye	0.634	0.152	−0.046	0.665	0.271	−0.166	0.498	0.014	−0.005
Guangzhou	0.710	0.285	−0.110	0.464	0.284	0.227	0.595	0.031	−0.021
Hefei	0.771	0.240	−0.119	0.358	0.411	0.218	0.256	0.032	−0.005
Chengdu	0.817	0.339	−0.291	0.850	0.329	0.276	0.702	0.036	−0.021

3.2. Validation of MEERA-2 AE with SONET

The validation results of MERRA-2 AE (440/870 nm) with SONET 12 sites are present in Figure 4. Generally, MERRA-2 AE show good performance with SONET ground-based measurements over all 12 sites. The MERRA-2 AE fits the one-to-one line for most of the sites. About 83.82% of matchup pairs are within the EE lines (+/−0.3) at Minqin site, where dust is the dominant source, and the correlation coefficient is 0.733, RMSE of 0.227, and bias of 0.005. In contrast, MERRA-2 AE is slightly overestimated at the Guangzhou urban site with high relative humidity. It may be due to the fact that there are high uncertainties in modeling anthropogenic aerosol sources and its hydroscopic growth. The MAE of AE that provides further quantitative illustration of the overestimation for fine mode aerosol particles at Guangzhou site. The MAEs over urban sites Nanjing, Shanghai, and Guangzhou are over 0.2. It implies that MERRA-2 tends to report smaller sizes of fine mode aerosols than SONET observations.

As shown in Figure 5a, the Chengdu and Guangzhou sites have higher AE (1.14 and 1.32), while Zhangye and Minqin sites have lower AE averages (0.55 and 0.66). As Figure 5b the Hefei and Chengdu sites have the largest MAE (both 0.30) for AE. Minqin has the smallest MAE (0.17). As Figure 5c shows the PDF of SONET and MERRA-2 AE, the statistical performance of the MERRA-2 is generally consistent with SONET (bias = 0.079). The PDFs of the AE difference (Figure 5d) show a normal distribution shape between −1~1.

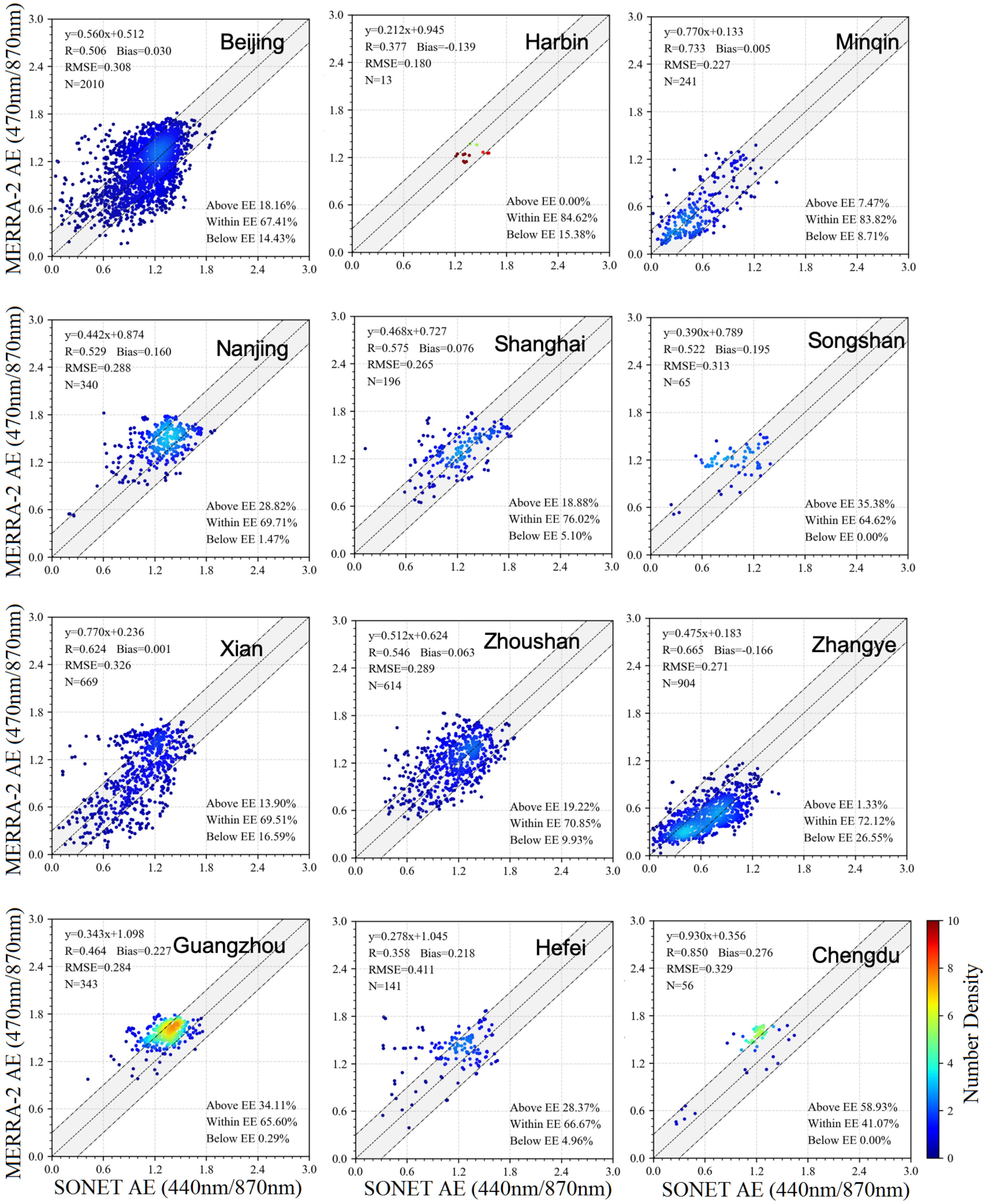

Figure 4. Same as Figure 2, but for AE.

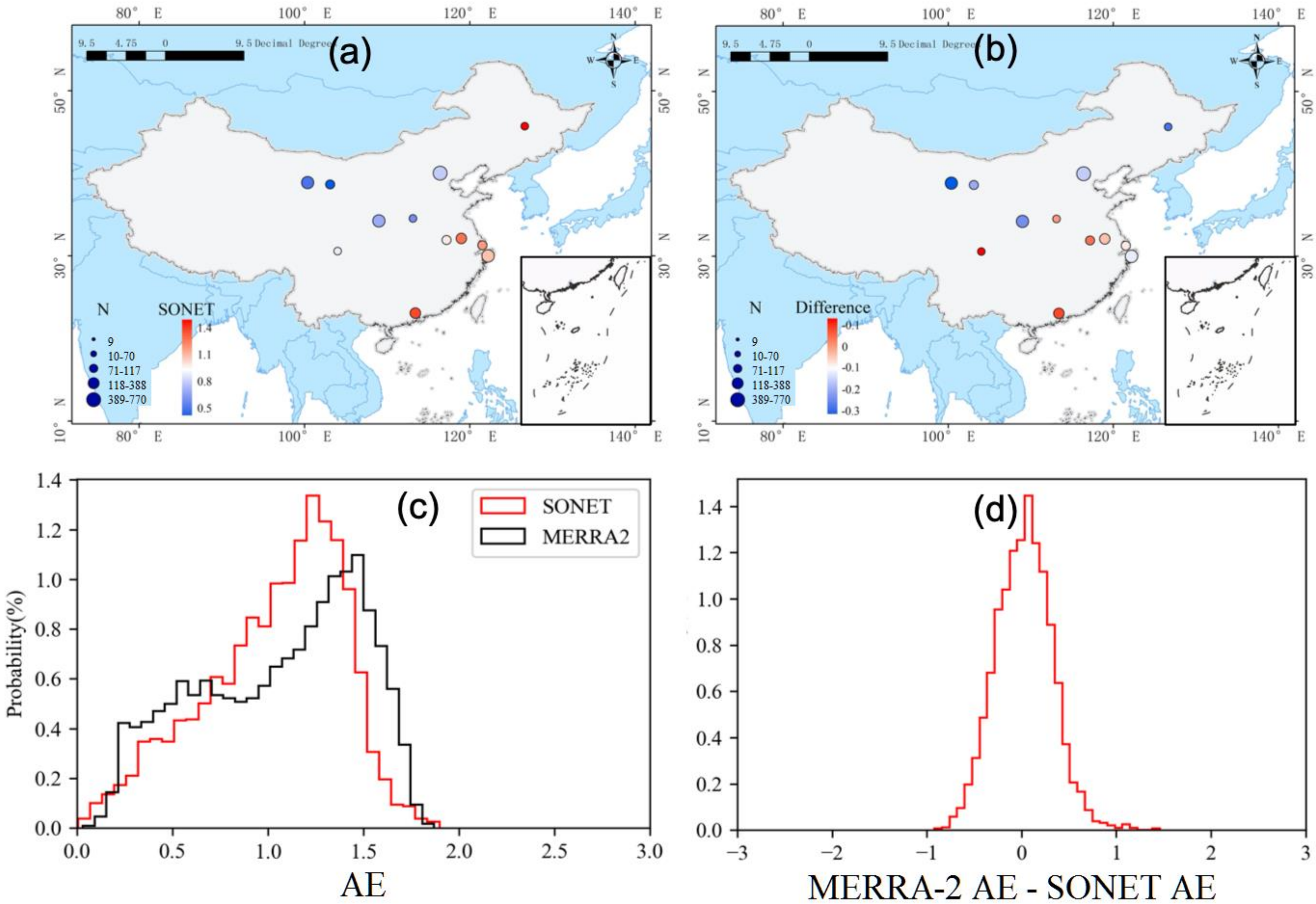

Figure 5. Same as Figure 3, but for AE.

3.3. Validation of MEERA-2 AAOD with SONET

Figure 6 shows the validations of MERRA-2 AAOD with SONET 12 sites over China. The results show that the MERRA-2 AAOD is of reasonable agreement with SONET, and the MERRA-2 AAOD is smaller than SONET over most of the sites. The maximum bias (MERRA-2 minus SONET) is 0.021. At the Beijing site, there are about 37.4% matchup pairs within the EE lines (+/−0.01+/−10%AAOD). It shows that MERRA-2 underestimates strongly in urban sites (Nanjing, Xian, Guangzhou, Chengdu, and Beijing), which may imply the underestimation of urban aerosol absorption. In addition, the urban sites are of relatively high AOD, therefore it may link with the underestimation of high AOD observed in Section 3.1. On the contrary, for the coastal site (Zhoushan), where the aerosol absorption is observed to be small, while MERRA-2 tends to slightly overestimate.

As shown in Figure 7a, the Chengdu and Xi'an sites show the highest annual AAOD (0.08), while Zhangye and Zhoushan sites are the lowest (0.026 and 0.027). As in Figure 7b, the Xi'an site shows the largest MAE (both 0.04). The Zhangye site is of the smallest MAE (0.01). Figure 7c shows the AAOD PDFs of SONET and MERRA-2. The statistical performance of the MERRA-2 is similar with SONET, and the MERRA-2 peak is slightly shifted to small values. The PDFs (Figure 7d) of AAOD difference reveal a normal distribution.

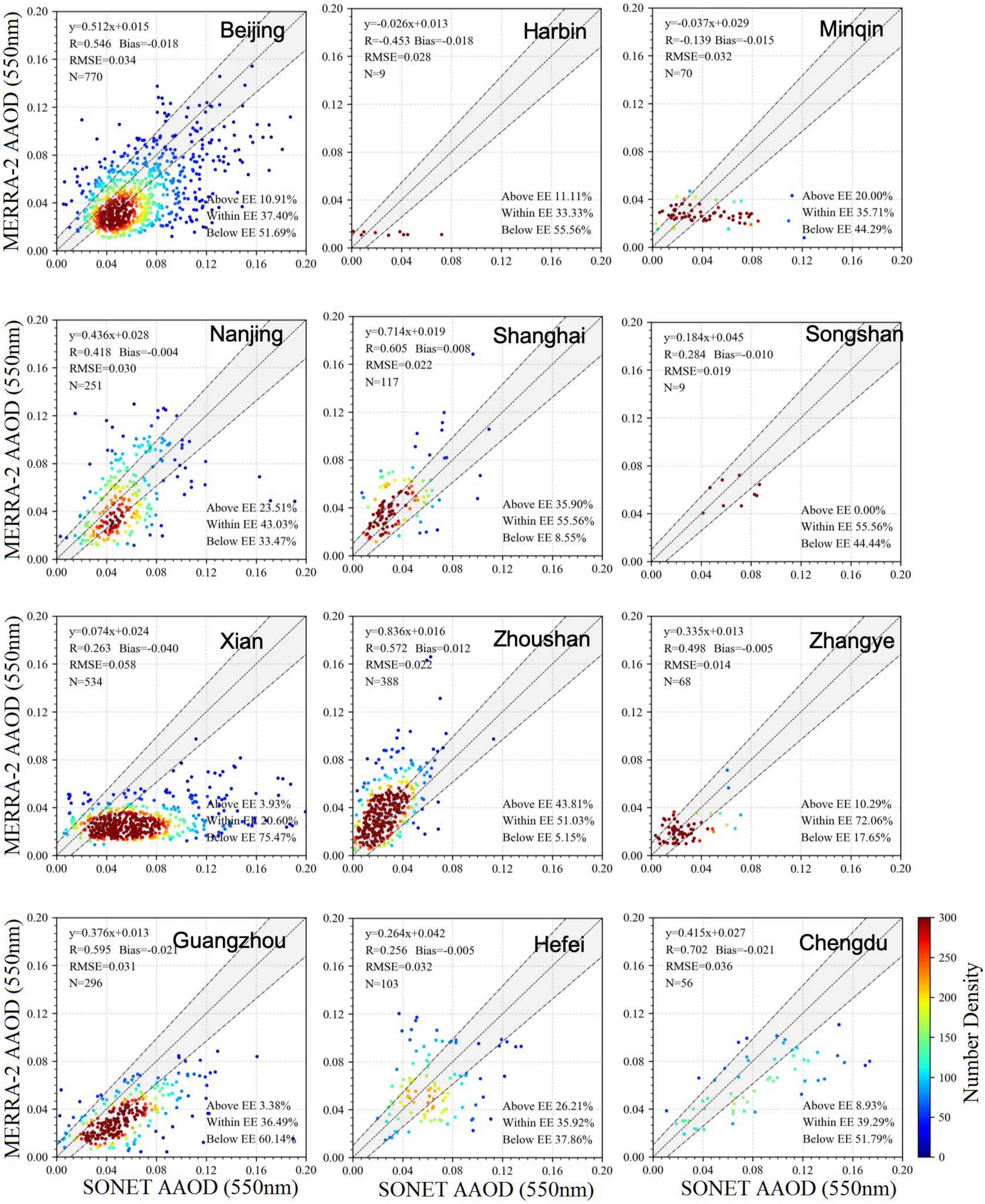

Figure 6. Same as Figure 2, but for AAOD.

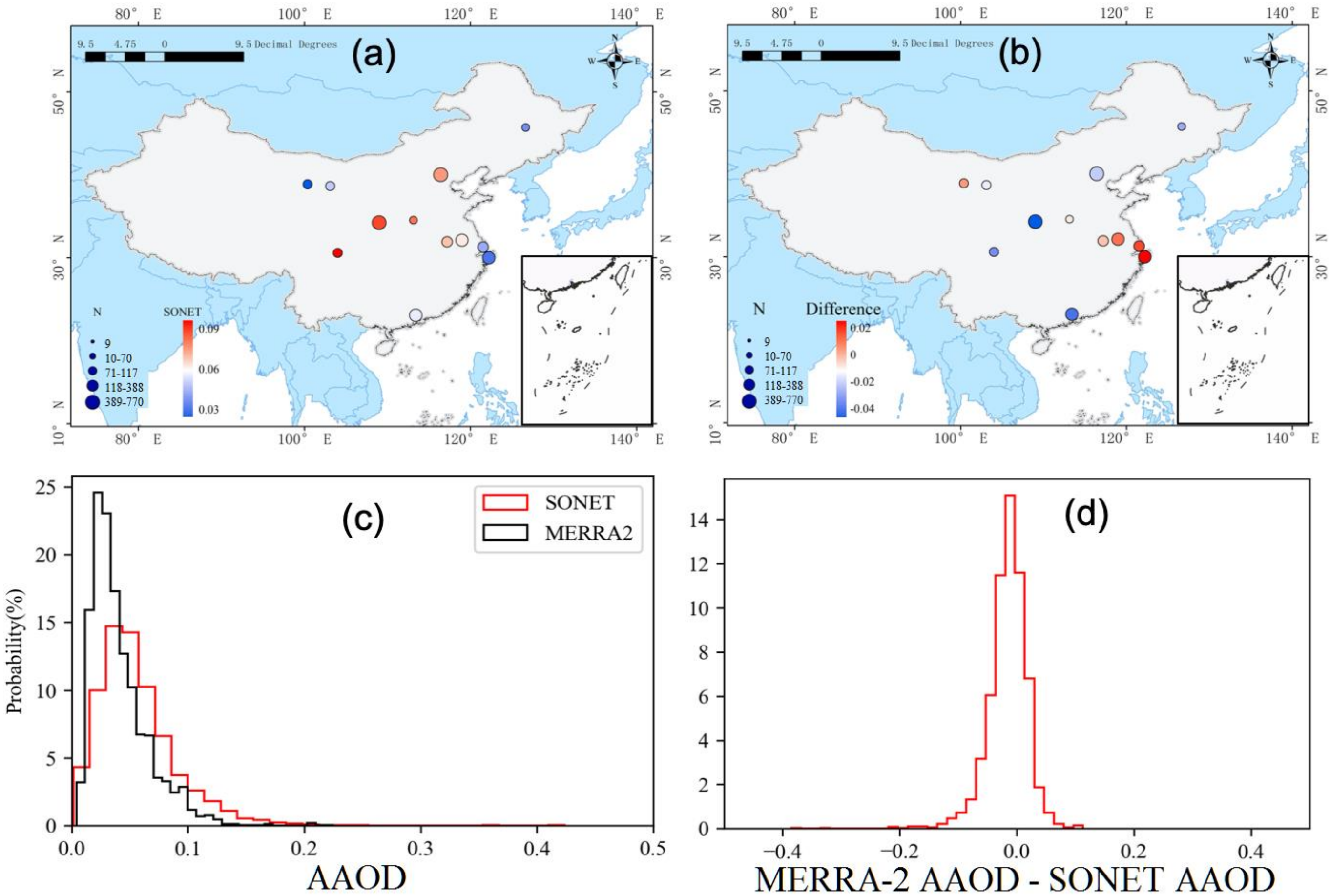

Figure 7. Same as Figure 3, but for AAOD.

3.4. Intercomparison of MERRA-2 and PARASOL Seasonal AOD

In this section, we intercompare pixel-by-pixel MERRA-2 seasonal AOD with PARASOL/GRASP. DJF represents the first quarter, winter (December, January and February); MAM is the second quarter, spring (March, April and May); JJA is the third quarter, summer (June, July and August); and SON is the fourth quarter, autumn (September, October and November). We use MERRA-2 monthly product (column concentration) to calculates the seasonal mean. We use PARASOL/GRASP "Models" Level 3 0.1 degree gridded seasonal products (https://www.grasp-open.com/products/ (accessed on 1 January 2022) and PARASOL/GRASP 0.1 degree data is resampled into MERRA-2 0.625 $\times$ 0.5 grid.

Figure 8 shows intercomparison of MEERA-2 seasonal AOD with PARASOL/GRASP over China. The results are presented season by season from 2011 to 2013. MERRA-2 shows good agreement with PARASOL/GRASP seasonal AOD, the correlation coefficient is at least 0.7 and RMSE is smaller than 0.16. The R is highest (0.864) in Autumn 2011, and it is smallest (0.743) in Summer 2012. In particular, the within EE of SON (Autumn) is relatively high, ranging from 72% to 84% in three years. From 2011 to 2013, both MERRA-2 and PARASOL/GRASP show slightly increasing AOD trends over China (Table 3). With the increase in AOD, MEERA-2 seems to show more pixels below EE with PARASOL/GRASP. Especially in 2013 MAM, MERRA-2 below EE fraction is approximately 15.5% with respect to PARASOL/GRASP products. The maximum value below EE fraction is in 2012 DJF Winter (21.93%).

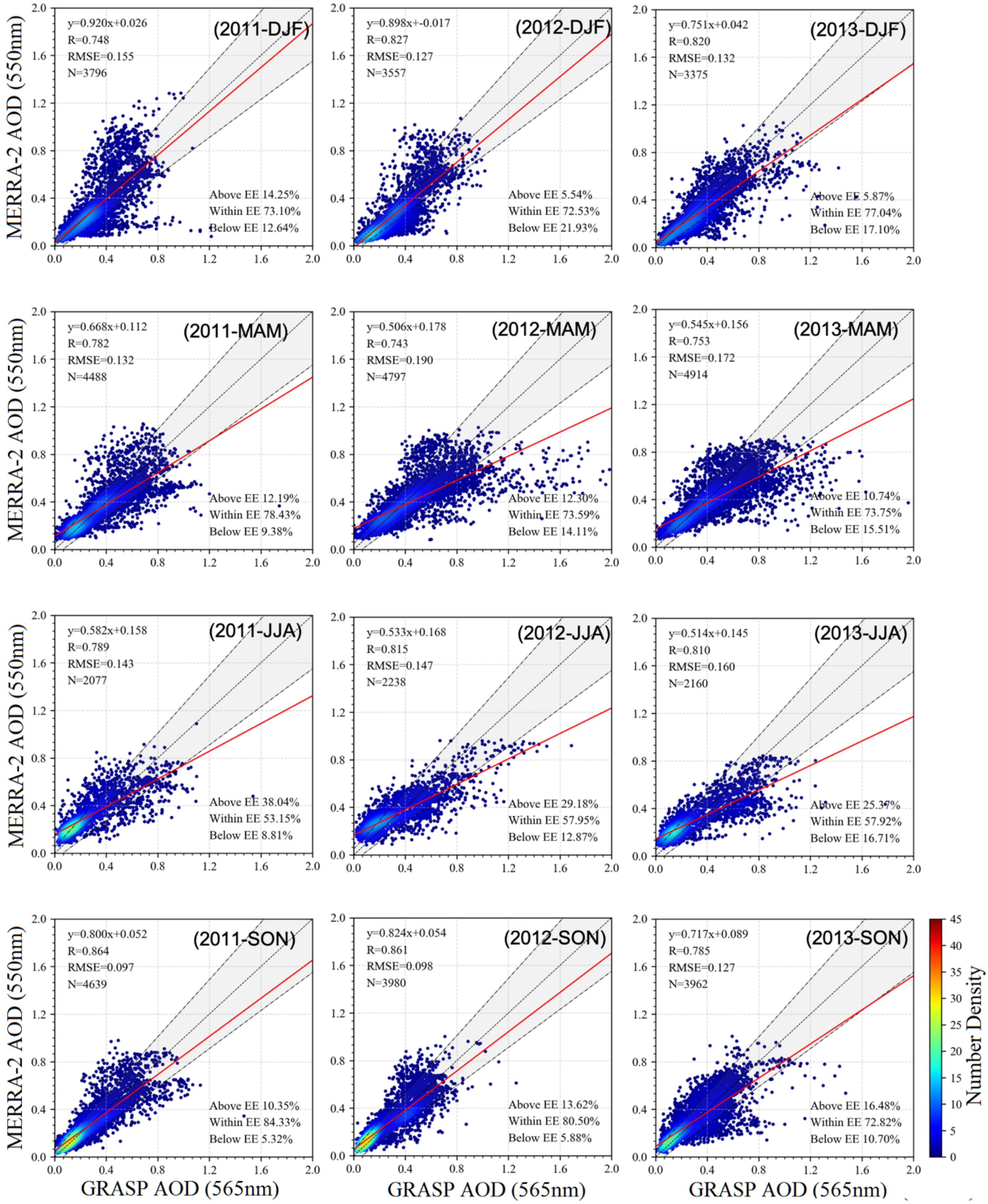

Figure 8. Intercomparison MERRA-2 seasonal AOD with PARASOL/GRASP "Models" over China. The grey dashed line represents the one-to-one line and EE line. The red, solid line represents the fitting line.

Figure 9 shows the spatial distribution of 2011–2013 seasonal AOD from MERRA-2 and PARASOL/GRASP over China. The high AOD is observed in Beijing, Tianjin, Hebei, PRD, and YRD regions. This is mainly due to the strong human activities in these regions. In central and eastern China, especially in densely populated areas, there are also high aerosol loading such as Sichuan basin. This probably causes MERRA-2 to underestimate the AOD value in the North China Plain due to the lack of nitrate considerations in the model, and the GOCART chemistry module contains only dust, sea salt, sulfate, black carbon, and organic carbon aerosol types. The MERRA-2 reanalysis data underestimation is affected by few factors: (i) GOCART model assumes external mixing of aerosol species, which limits its ability to simulate overmixed species of aerosol; (ii) the MERRA-2 anthropogenic input uses monthly dataset which is of time lag; (iii) and the assimilated MODIS AOD is underestimated over China.

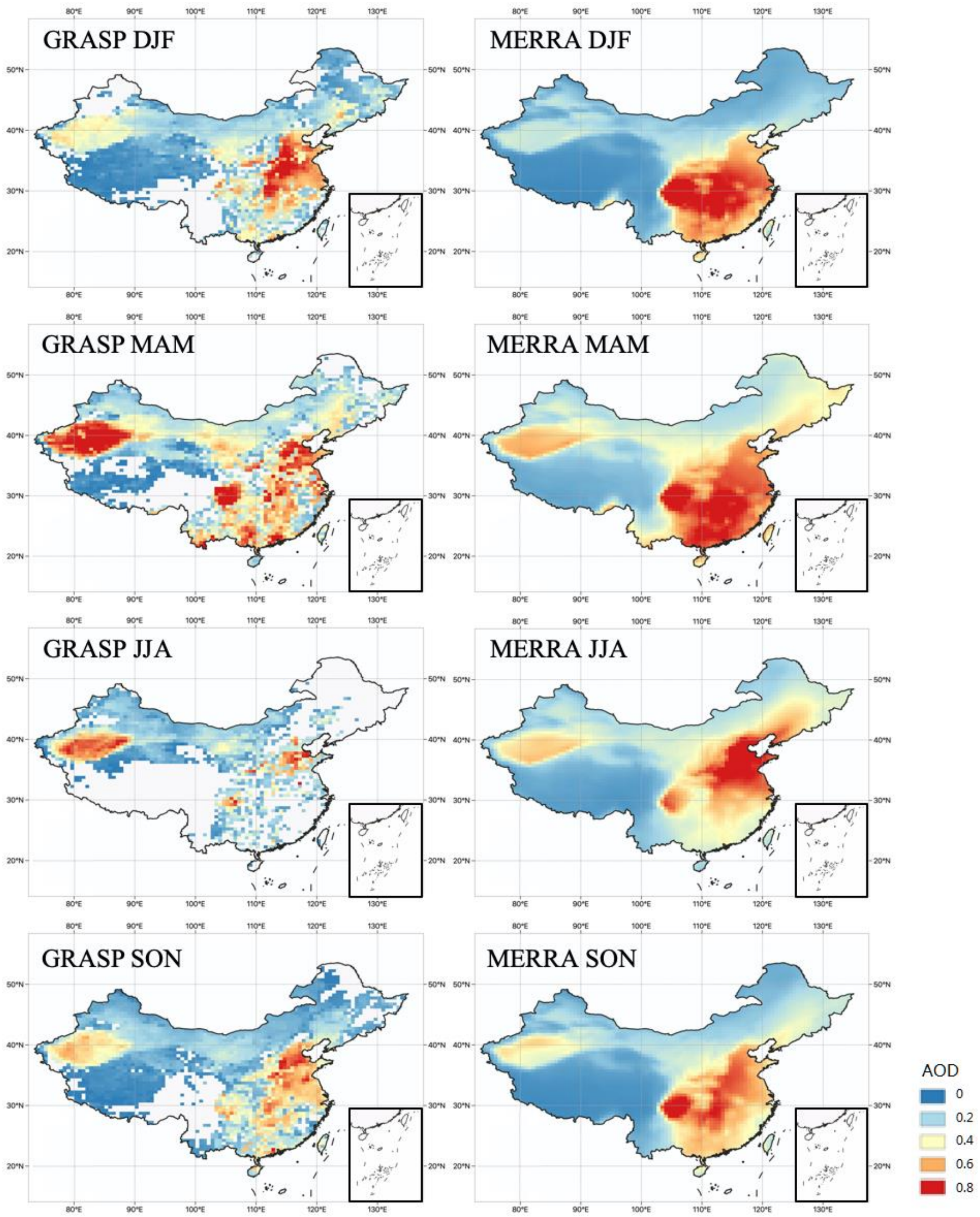

Figure 9. Spatial distribution of 2011–2013 seasonal AOD from MERRA-2 and PARASOL/GRASP over China.

Table 3. The statistics mean of the seasonal values for MERRA-2 and GRASP from Jan 2011 to Dec 2013.

	MERRA-2					GRASP				
	AOD	**AE**	**AAOD**	**BC(mg/m^3)**	**DU(mg/m^3)**	**AOD**	**AE**	**AAOD**	**BC(mg/m^3)**	**DU(mg/m^3)**
2011_DJF	0.109	0.860	0.004	0.388	23.228	0.239	0.882	0.038	1.115	93.975
2011_MAM	0.130	0.790	0.006	0.433	46.267	0.264	0.809	0.038	0.459	166.719
2011_JJA	0.131	0.848	0.006	0.498	43.907	0.284	0.868	0.038	0.699	162.528
2011_SON	0.117	0.904	0.006	0.582	25.467	0.237	0.986	0.033	1.127	77.576
2011	0.122	0.851	0.006	0.475	34.717	0.256	0.886	0.037	0.850	125.200
2012_DJF	0.112	0.828	0.005	0.460	26.850	0.264	0.871	0.039	1.197	105.171
2012_MAM	0.137	0.748	0.007	0.465	52.986	0.320	0.787	0.040	0.624	197.509
2012_JJA	0.131	0.843	0.007	0.529	40.686	0.300	0.867	0.040	0.819	181.122
2012_SON	0.109	0.907	0.006	0.537	21.895	0.232	0.936	0.033	1.213	80.796
2012	0.122	0.832	0.006	0.498	35.604	0.279	0.865	0.038	0.963	141.149
2013_DJF	0.107	0.802	0.005	0.416	23.691	0.245	0.850	0.038	1.254	95.657
2013_MAM	0.124	0.743	0.006	0.430	44.754	0.277	0.809	0.037	0.863	156.082
2013_JJA	0.123	0.833	0.006	0.496	39.006	0.310	0.867	0.042	0.863	156.082
2013_SON	0.103	0.857	0.005	0.449	22.714	0.260	1.080	0.022	1.159	157.360
2013	0.114	0.809	0.005	0.448	32.541	0.273	0.901	0.035	1.086	91.028
2011–2013	0.119	0.830	0.006	0.474	34.288	0.269	0.884	0.037	0.966	119.126

3.5. Intercomparison of MERRA-2 and PARASOL Seasonal AE

Previous study has shown the good performance of PARASOL/GRASP detailed aerosol properties, such as AE, SSA, AAOD, etc. [22]. Here we intercompared pixel-by-pixel MERRA-2 and PARASOL/GRASP seasonal AE, as shown in Figure 10. For MERRA-2, the up limit of AE seems to be 1.5. A good agreement is observed for two products, almost all seasons are of at least 50% EE fraction (+/−0.3), and the agreement is generally better in MAM (spring) and JJA (summer) with at least 70% EE fraction than that of DJF (winter) ~40–50% and SON (autumn) ~50–70%. MERRA-2 shows smaller particles with higher AE than PARASOL/GRASP, about 65% of sites with at least 20% above EE fraction. In China, MAM is of dry weather, high wind speed, and strong cold air and is easily affected by desert dust. The content of coarse particles is relatively large, and the AE value is relatively small; The secondary transformation of the aerosol particles promotes the formation of secondary aerosols and the formation of large particles, and the AE value decreases; the cold air invasion temperature is low in autumn and winter, and the ice and snow covering the surface is not conducive to the entry of coarse-particle soil aerosols into the atmosphere. Material burning and burning heating make the AE value relatively high.

Figure 11 shows the spatial distribution of 2011–2013 seasonal AE from MERRA-2 and PARASOL/GRASP over China. MERRA-2 is generally higher than PARASOL/GRASP and indicates smaller particles. Meanwhile, we also found the fine mode aerosol concentered in Eastern China densely populated areas. In the Taklimakan Desert, the AE from both products are very small. On one hand, the reanalysis dataset is of the full coverage, but on the other hand the observational dataset provides higher accuracy. Therefore, the evaluation of the reanalysis dataset with independent observational products could provide more insights.

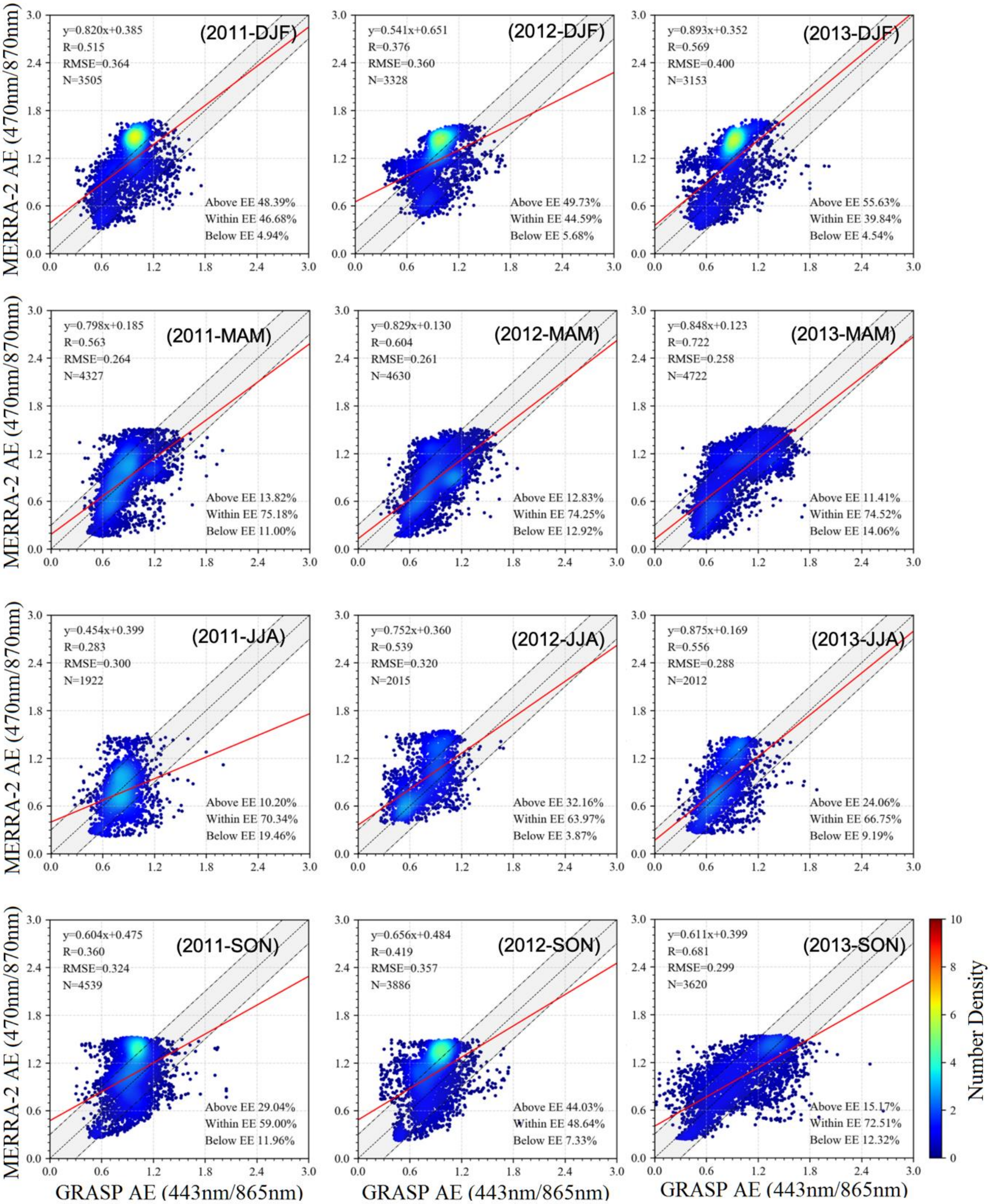

Figure 10. Same as Figure 6, but for AE.

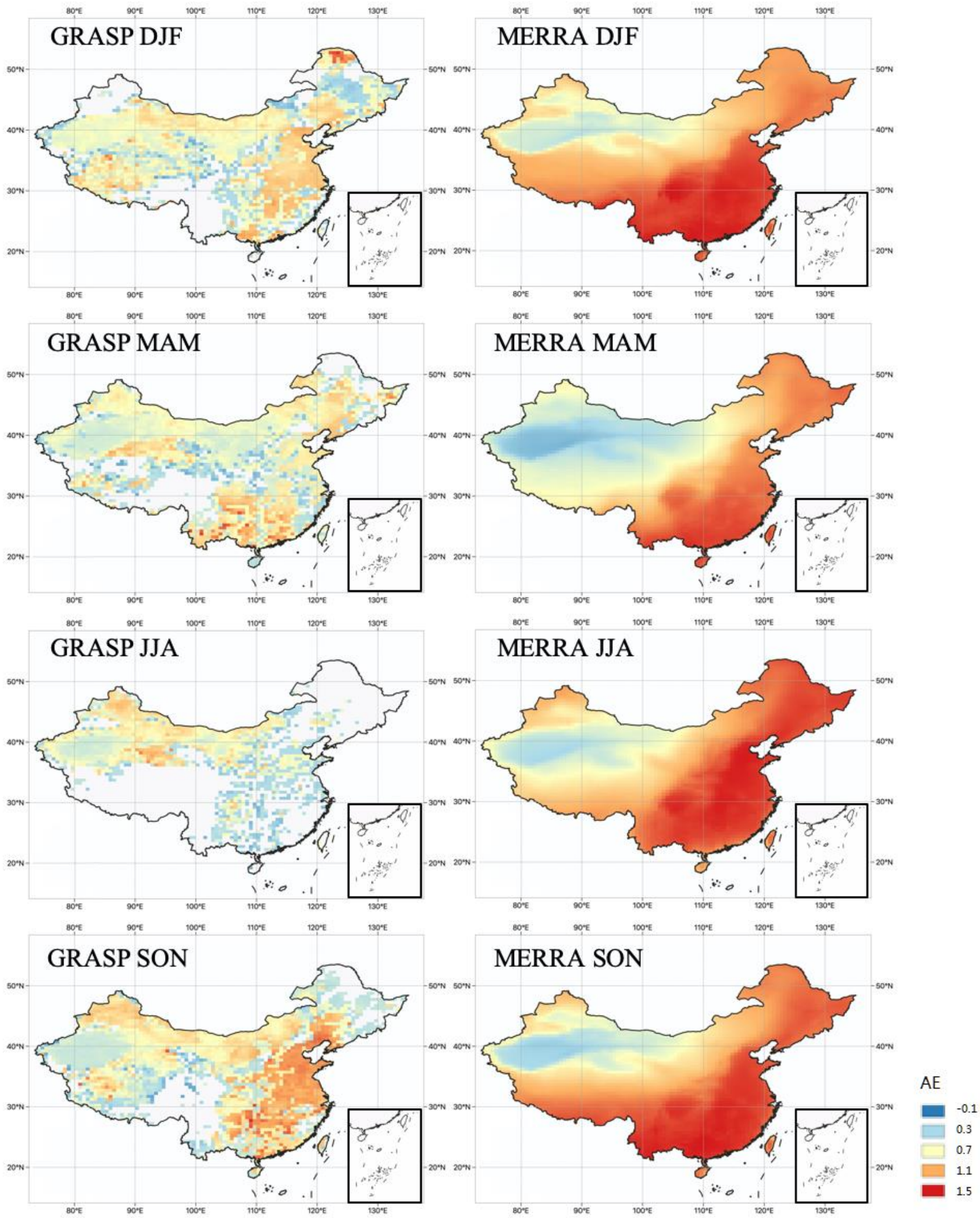

Figure 11. Same as Figure 9, but for AE.

3.6. Intercomparison of MERRA-2 and PARASOL Seasonal AAOD

We intercompared pixel-by-pixel MERRA-2 and PARASOL/GRASP seasonal AAOD in Figure 12. The MERRA-2 AAOD is calculated by subtracting the scattering AOD from the total. Even though MERRA-2 shows similar spatial distribution (Figure 13) to PARASOL/GRASP, MERRA-2 AAOD is clearly smaller than PARASOL/GRASP. This is consistent with the validation results with SONET that MERRA-2 underestimates AAOD over China (bias = −0.011). The RMSE varies from 0.013 to 0.033 from season to season. The underestimation in spring and summer is more significant than that in autumn and winter. Moreover, the spatial distribution of AAOD is similar to that of AOD. The high AAOD is also observed in regions with high human activities.

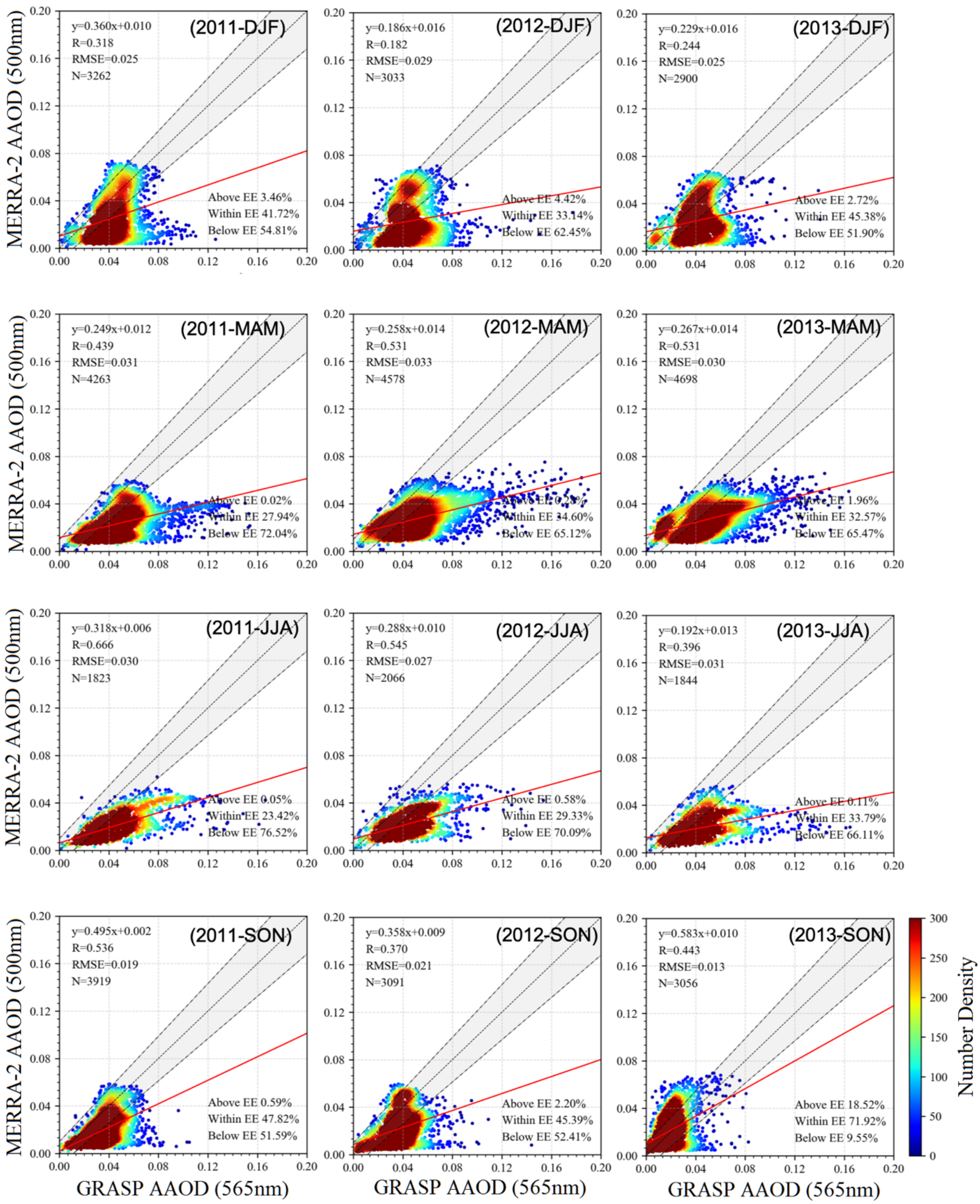

Figure 12. Same as Figure 6, but for AAOD.

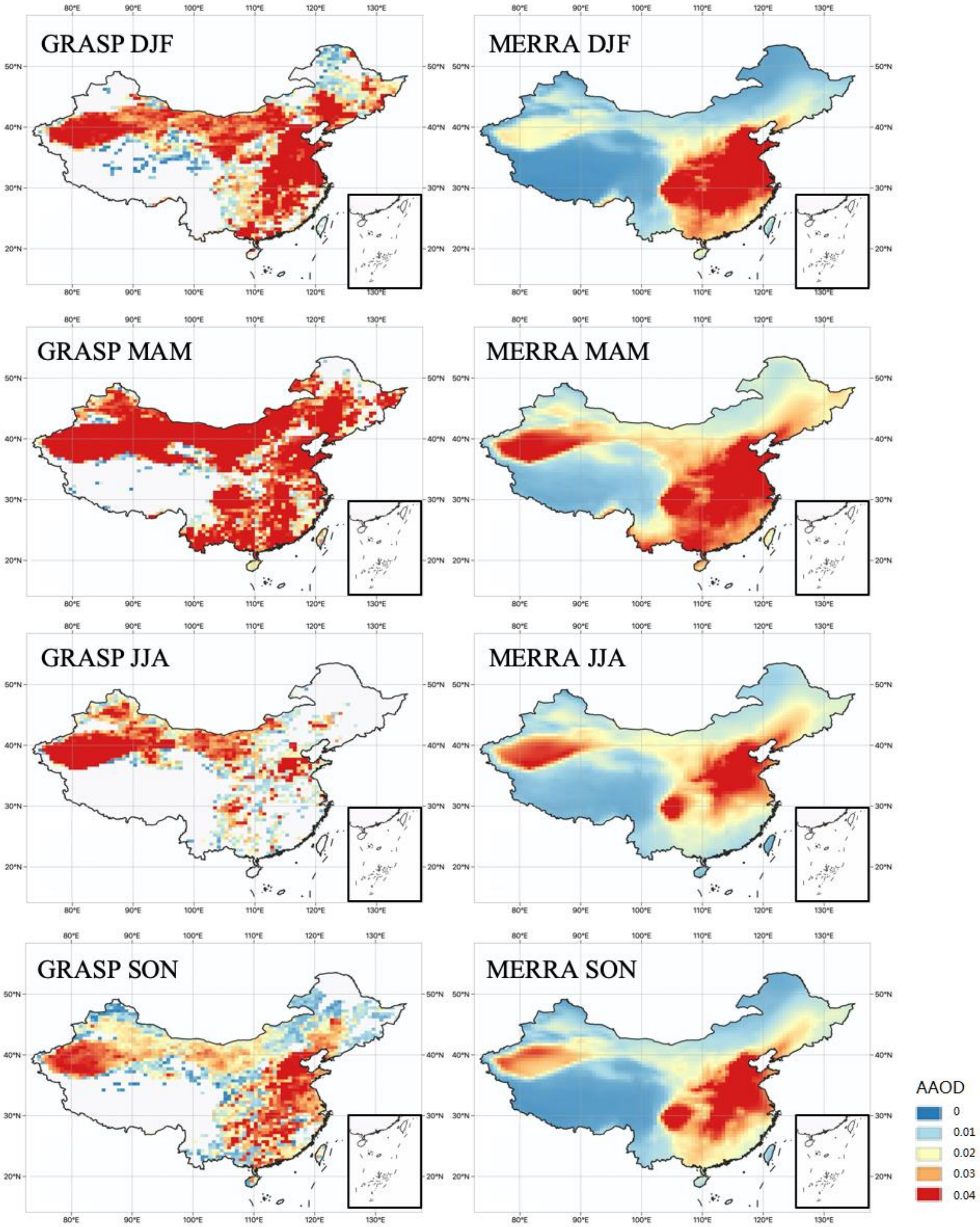

Figure 13. Same as Figure 9, but for AAOD.

4. Discussion

4.1. Climatological Aerosol Optical Propertie

Figure 14 shows the spatial distribution of climatological (2011–2013) MERRA-2 and PARASOL/GRASP AOD (550 nm), AE (440/870), and AAOD (550 nm) over China. Both AOD and AAOD are of good agreement spatially. The high AOD values are mainly in the NCP, YRD, and the Sichuan Basin with AOD > 0.8. The maximum value of AOD of MERRA-2 is 0.8 which is close to the PARASOL/GRASP AOD. A similar phenomenon is also shown in the spatial distribution of AAOD. But the AAOD of PARASOL/GRASP on Inner Mongolia was slightly higher than MERRA-2. This result is basically the same as the previous research obtained by using satellite, e.g., MODIS, etc. Due to the complicated terrain (restricted diffusion) and special climate (high relative humidity) in the Sichuan Basin, the annual AOD over this area is relatively high. On the NCP and YRD, anthropogenic pollution is the dominant source. The high AOD in the Taklimakan desert areas of Xinjiang in western China is mainly affected by dust aerosol. AOD is relatively low in the Northeast and Qinghai-Tibet Plateau with annual mean AOD < 0.4. Overall, the spatial distribution of AAOD is similar to that of AOD. Meanwhile, the MERRA-2 AE can clearly reflect qualitatively that the particle size in eastern China is small mainly fine particles, and the AE in desert areas is smaller mainly coarse particles, while the AE result of the PARASOL/GRASP satellite has a relatively small dynamic range with respect to MERRA-2 which is due to the limitation of «models» datasets. The AE of MERRA-2 is larger than that of PARASOL/GRASP when fine particles dominate, which is consistent with the validation in Section 3.2 that MERRA-2 tends to underestimate fine particle size in particular over urban areas.

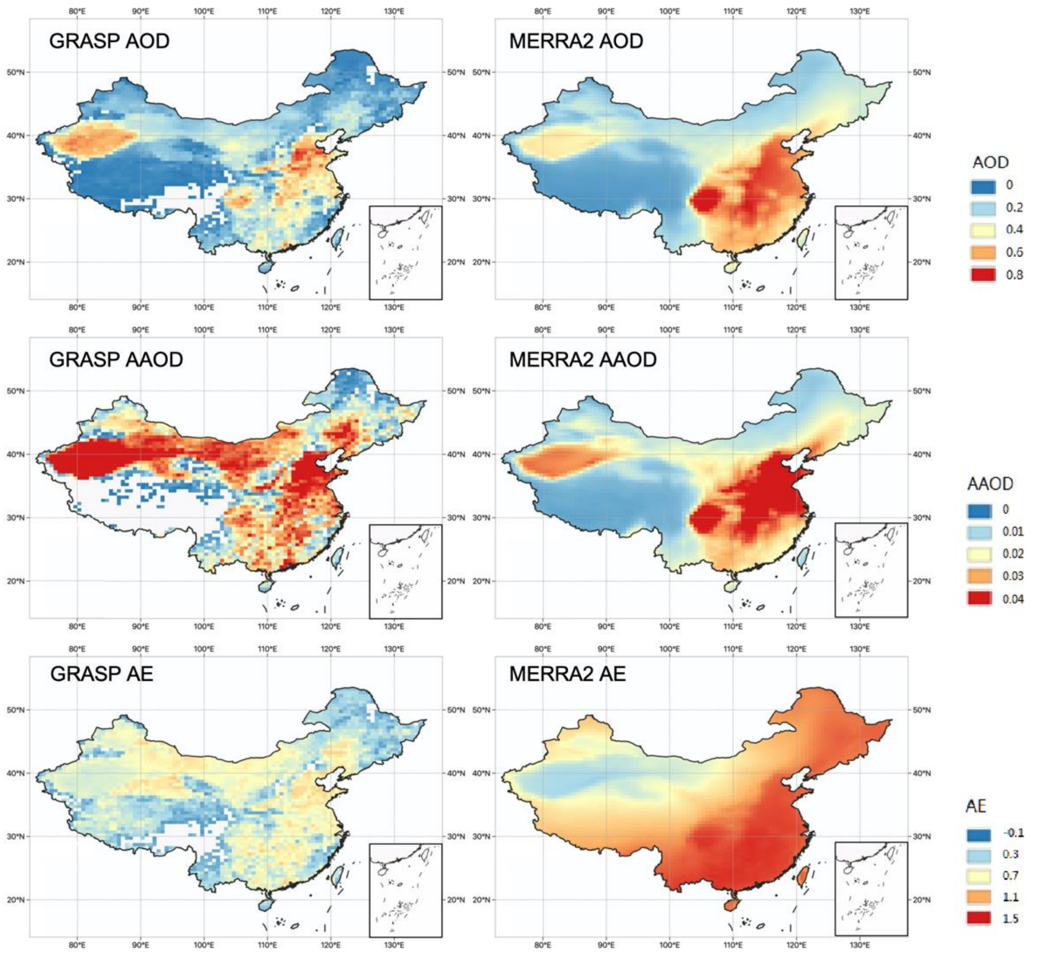

Figure 14. Spatial distribution of 2011–2013 climatological aerosol optical properties from PARASOL/GRASP and MERRA-2. The PARASOL/GRASP data is resampled to MERRA-2 $0.625 \times 0.5°$ resolution.

4.2. Climatological Aerosol Components

With the Maxwell–Garnett effective medium approximation, the PARASOL/GRASP «components» approach derive aerosol optical properties together with aerosol components' columnar concentration [29]. This is because the aerosol components of GRASP «components» approach is defined based on the sensitivity to the optical remote sensing observations, and they are not the same as MERRA-2 species. Therefore, we will compare black carbon (BC) and dust (DU) which are of similar definition in both products. Specifically, we compare 'Soot_Volume_Concentration_F' in GRASP/components with MERRA-2

BC, and 'nonabsorbing insoluble' in GRASP/components with MERRA-2 DU. Although the BC content in aerosols is very small, its impact on climate change and human health is significant [41]. Figure 15 shows that the spatial distribution of MERRA-2 and PARASOL/GRASP climatological (2011–2013) BC and DU columnar concentration. In general, they are in good agreement with many spatial similarities. The areas with a high average annual distribution of BC are mainly located in the NCP, East China Region and Sichuan Basin, where industrial emissions are dominant. MERRA-2 and PARASOL/GRASP show columnar BC concentration between 1.5–2 mg/m^3. The low value is observed in northeastern and western China, with an average BC value lower than 0.5 mg/m^3. In addition, dust aerosols, as the most abundant components in the atmosphere, mainly come from natural sources. As shown in Figure 15, the dust contents are high near the desert and its downwind region and low in other areas. The highest dust columnar concentration in China is observed in the Taklimakan Desert. The mean dust columnar concentration is as high as 150 mg/m^3. The dust aerosol content in southern China is lower than 30 mg/m^3. Even though, both MERRA-2 and PARASOL/GRASP show high dust concentration over the downwind region (NCP), PARASOL/GRASP tend to report higher dust concentration there, which can be due to the missing of small scale on-road dust emission in the MERRA-2 model [42].

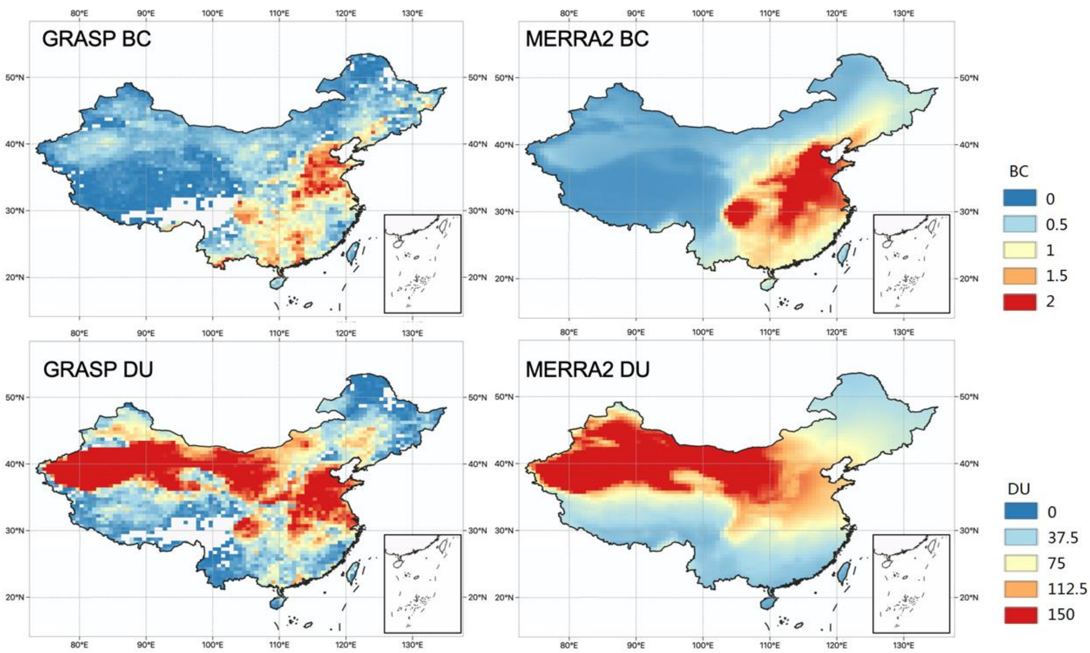

Figure 15. Spatial distribution of 2011–2013 climatological BC and DU columnar concentrations from PARASOL/GRASP and MERRA-2. The PARASOL/GRASP data is resampled to MERRA-2 $0.625 \times 0.5^{\circ}$ resolution.

4.3. Evaluation of BC Mass Concentration with In situ Measurements

A previous study by Li et al. [43] evaluated PARASOL/GRASP BC mass concentration with in situ measurements and showed reasonable agreement. Here, we further use the in-site BC measurements from AE-51 at Beijing to evaluate PARASOL/GRASP satellite retrieval and MERRA-2 reanalysis products in October 2012. Figure 16 shows a time series of the daily average value from AE-51, MERRA-2, and PARASOL/GRASP. The AE-51 measured value is the mass concentration of BC near the ground obtained by the black carbon meter AE-51 using a time-matching window of 15 min. The inverted value is based on the formula using the inverted black carbon volume proportion, the total volume of aerosol, and the mass density of black carbon (ρ_{BC} = 1.8 g/cm^3) to obtain the BC mass concentration. In particular, the result of PARASOL/GRASP represents the BC content in the entire atmospheric column, while AE-51 observes the concentration of BC on the ground level. We are making absolute comparisons and need to convert the two into a unified vertical space range. Here, we assume that the atmospheric boundary layer height PBLH is 1 km.

$$C_{m,i} = \rho_{m,i} \cdot f_i \cdot V_{total} = \rho_{m,i} \cdot f_i \cdot \int_{r_{min}}^{r_{max}} \frac{dV}{dlnr} dlnr, \tag{7}$$

$$\mathrm{BC}_{\mathrm{surface,estimation}} = \frac{\mathrm{BC}_{\mathrm{column,retrieval}}}{\mathrm{PBLH}}, \tag{8}$$

where $C_{m,i}$ is the columnar mass concentration of the i-th component, which is the mass concentration of the aerosol component in the total atmosphere per unit area (unit: mg/m^2), $\rho_{m,i}$ is the mass density of the *i*-th component [44], V_{total} is the total aerosol volume, f_i is the volume fraction of the *i*-th component. r_{max} and r_{min} represent the maximum and minimum radius of aerosol volume size distribution, respectively.

It can be seen that the time series trends of the AE-51 BC measurements, PARASOL/GRASP retrieval, and the MERRA-2-modelled BC at the surface level are in reasonable agreement. In some case, when the BC concentration is low, the PARASOL/GRASP retrieval value is more consistent with the observation, especially in 22 October 2012, where the difference between PARASOL/GRASP retrieval value and AE-51 BC measurements is nearly zero. However, in 22 October 2012, PARASOL/GRASP clearly underestimate BC, which may be caused by the error of the retrieval itself or the assumption of 1 km PBLH to convert columnar BC to near surface [43]. This phenomenon was also found in Lei et al. [43]. The MAEs of MERRA-2 and GRASP are 0.44 and −0.38, respectively, with respect to the AE-51 measurements. PARASOL/GRASP BC is slightly underestimated, and MERRA-2 BC is slightly overestimated relative to the observed value.

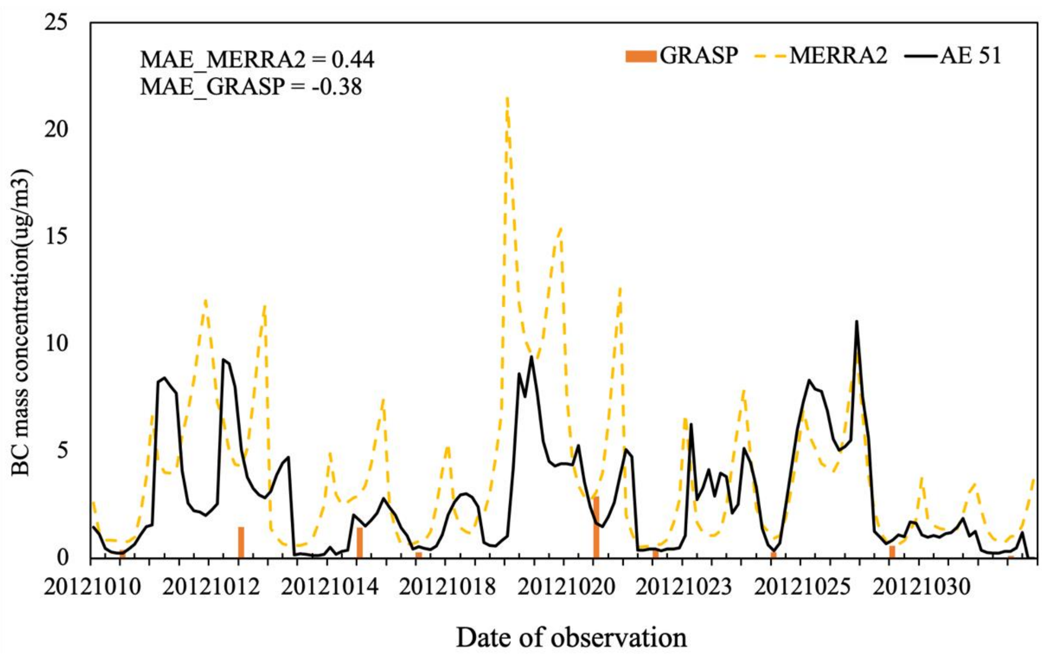

Figure 16. Evaluation of near surface BC mass concentration from MERRA-2 and PARASOL/GRASP with in situ measurements at Beijing.

5. Conclusions

The validation results with SONET ground-based sun-photometer measurements show that the MERRA-2 AOD are of good agreement with SONET at 12 sites, R = 0.634–0.822 and RMSE = 0.118–0.339. The highest R is observed at coastal site Zhoushan (0.822), and the lowest R is at rural site Zhangye (0.634). The Xi'an and Chengdu urban sites are of the highest bias AOD (−0.29). Overall, MERRA-2 AOD is slightly underestimated about 0.22 over China.

The validation of AE show that the MERRA-2 AE are of good agreement with SONET at 12 sites, R = 0.358–0.850 and RMSE = 0.180–0.411. The highest R is observed at basin site Chengdu (0.850), and the lowest R is at rural site Hefei (0.358). The Chengdu urban site is of the highest bias AE (0.276). Totally, MERRA-2 AE is a certain degree of relaxed consistent with SONET over China.

The results of AAOD show that the MERRA-2 AAOD are underestimated with SONET at 12 sites, R = −0.453–0.702 and RMSE = 0.014–0.058. The highest R is observed at basin site Chengdu (0.702), and the lowest R is at urban Harbin (−0.453). The Xi'an urban site is of the highest bias AAOD (−0.040). On the whole, MERRA-2 AAOD is generally more underestimated, about 0.008 over China.

The seasonal MERRA-2 AOD, AE, and AAOD are pixel-by-pixel evaluated with PARASOL/GRASP products. The spatial distribution is consistent in that the high AOD is observed over NCP, PRD, YRD, and Sichuan Basin, where anthropogenic activities are high, as well as Taklimakan Desert. In terms of seasonal variation, AOD is the highest in summer, followed by spring, autumn and winter. AAOD is of similar seasonal changes as AOD. AE is the highest in winter, followed by summer and autumn and spring.

Furthermore, the PARASOL/GRASP «components» BC and DU products are used to evaluate MERRA-2 BC and DU spatial distribution. Over east China's industrial regions (NCP, PRD, YRD, and Sichuan Basin), both MERRA-2 and PARASOL/GRASP show a high columnar BC mass concentration 1.5–2 mg/m^3, and MERRA-2 is slightly higher than PARASOL/GRASP. The climatological dust mass concentration is also in such good agreement that the high value (~150 mg/m^3) is observed near the Taklimakan Desert. Meanwhile, over the downwind region, MERRA-2 reports lower dust concentration than PARASOL/GRASP, which could be the missing small-scale on-road dust missions. The dust aerosol mass concentration in southern China is relatively low, usually below 30 mg/m^3. We also utilize the in situ BC measurements at Beijing to evaluate one-month time series PARASOL/GRASP and MERRA-2 near-surface BC mass concentration. Generally, MERRA-2 well captures the daily variation and is a bit overestimated (MAE = +0.44 $\mu g/m^2$), and PARASOL/GRASP is slightly underestimated (MAE = −0.38 $\mu g/m^2$) especially for high BC cases.

Even though some issues are identified, such as underestimation of high AOD, aerosol absorption, overestimation of fine mode aerosol AE, slightly overestimation of BC mass, etc., the MERRA-2 reanalysis dataset shows overall reasonable agreement with independent measurements from SONET, PARASOL/GRASP and in situ measurements. We want to emphasize the two advantages (i) full spatial coverage; (ii) temporal continuity of the reanalysis dataset. Satellite data has the advantage of high resolution, and reanalysis data has the advantage of time continuity. Therefore, multi-source multi-dimensional analysis are desired, since each dataset may have its own advantages and disadvantages and they complement each other.

Author Contributions: For research articles with several authors, Y.O. performed the validation and prepared the paper. Z.L. conceived on the paper. C.C. designed the study and modified the full text. Y.Z. provided advice on MERRA-2. K.L. and H.X. provided SONET data. Z.S. gave advice on the design of the figures of validation. J.D. provided advice on validation. Z.P. revised the language of the article. Y.X. provided the AE-51 data. J.L. gave advice on BC validation. All authors have read and agreed to the published version of the manuscript.

Funding: This work is supported by National Outstanding Youth Foundation of China (Grant No. 41925019) of Zhengqiang Li. This work is also supported by the National Natural Science Foundation of China (No. 42175147) of Y.X. and National Natural Science Foundation of China (No. 42101365) of Yuanyuan Wei. C. Chen also recognizes support by Open Fund of State Key Laboratory of Remote Sensing Science [Grant number OFSLRSS202008].

Informed Consent Statement: Informed consent was obtained from all subjects involved in the study.

Data Availability Statement: Not Applicable.

Acknowledgments: Thanks to the entire GRASP-OPEN (https://www.grasp-open.com/ (accessed on 1 Jauuary 2022)) team for the algorithm development. We are grateful to SONET sites for ground-based data, and to the MERRA-2 team of NASA.

Conflicts of Interest: The authors declare no conflict of interest. The funders had no role in the design of the study; in the collection, analyses, or interpretation of data; in the writing of the manuscript, or in the decision to publish the results.

References

1. Huang, R.J.; Zhang, Y.; Bozzetti, C.; Ho, K.F.; Cao, J.J.; Han, Y.; Daellenbach, K.R.; Slowik, J.G.; Platt, S.M.; Canonaco, F.; et al. High secondary aerosol contribution to particulate pollution during haze events in China. *Nature* **2014**, *514*, 218–222. [CrossRef] [PubMed]
2. Ramanathan, V.; Carmichael, G. Global and regional climate changes due to black carbon. *Nat. Geosci.* **2008**, *36*, 335–358. [CrossRef]
3. Reinman, S.L. Intergovernmental Panel on Climate Change (IPCC). *Encycl. Energy Nat. Resour. Environ. Econ.* **2013**, *26*, 48–56. [CrossRef]
4. Chen, S.C.; Liao, C.M. Health risk assessment on human exposed to environmental polycyclic aromatic hydrocarbons pollution sources. *Sci. Total Environ.* **2006**, *366*, 112–123. [CrossRef] [PubMed]
5. Deschamps, P.; Breon, F.; Leroy, M.; Podaire, A.; Bricaud, A.; Buriez, J.; Seze, G. The POLDER mission: Instrument characteristics and scientific objectives. *IEEE Trans. Geosci. Remote Sens.* **1994**, *32*, 598–615. [CrossRef]
6. Anderson, T.L.; Wu, Y.; Chu, D.A.; Schmid, B.; Redemann, J.; Dubovik, O. Testing the MODIS satellite retrieval of aerosol fine-mode fraction. *J. Geophys. Res.* **2005**, *110*, D18204. [CrossRef]
7. Gelaro, R.; Mccarty, W.; Suárez, M.; Todling, R.; Molod, A.; Takacs, L.; Randles, C.; Darmenov, A.; Bosilovich, M.G.; Reichle, R. Climate Data Guide—Modern Era Retrospective Analysis for Research and Applications, version 2 (MERRA-2). *J. Clim.* **2017**, *30*, 5419–5454. [CrossRef]
8. Cao, S.; Zhang, S.; Gao, C.; Yan, Y.; Bao, J.; Su, L.; Liu, M.; Peng, N.; Liu, M. A long-term analysis of atmospheric black carbon MERRA-2 concentration over China during 1980–2019. *Atmos. Environ.* **2021**, *264*, 118662. [CrossRef]
9. Ryu, Y.H.; Min, S.K. Long-term evaluation of atmospheric composition reanalyses from CAMS, TCR-2, and MERRA-2 over South Korea: Insights into applications, implications, and limitations—ScienceDirect. *Atmos. Environ.* **2020**, *246*, 118062. [CrossRef]
10. Wei, J.C. Characterize Aerosols from MODIS/MISR/OMI/MERRA-2: Dynamic Image Browse Perspective. In Proceedings of the Agu Fall Meeting, New Orleans, LA, USA, 13–17 December 2021.
11. Cheng, C.; Dubovik, O.; Schuster, G.L.; Fuertes, D.; Meijer, Y.; Landgraf, J.; Karol, Y.; Li, Z. Characterization of temporal and spatial variability of aerosols from ground-based climatology: Towards evaluation of satellite mission requirements. *J. Quant. Spectrosc. Radiat. Transf.* **2021**, *268*, 107627. [CrossRef]
12. Sun, E.; Che, H.; Xu, X.; Wang, Z.; Lu, C.; Gui, K.; Zhao, H.; Zheng, Y.; Wang, Y.; Wang, H. Variation in MERRA-2 aerosol optical depth over the Yangtze River Delta from 1980 to 2016. *Theor. Appl. Climatol.* **2019**, *136*, 363–375. [CrossRef]
13. Sun, E.; Xu, X.; Che, H.; Tang, Z.; Gui, K.; An, L.; Lu, C.; Shi, G. Variation in MERRA-2 aerosol optical depth and absorption aerosol optical depth over China from 1980 to 2017. *J. Atmos. Sol. Terr. Phys.* **2019**, *186*, 8–19. [CrossRef]
14. Tuygun, G.T.; Gündodu, S.; Elbir, T. Estimation of ground-level particulate matter concentrations based on synergistic use of MODIS, MERRA-2 and AERONET AODs over a coastal site in the Eastern Mediterranean. *Atmos. Environ.* **2021**, *261*, 118562. [CrossRef]
15. Molod, A.; Takacs, L.; Suarez, M.; Bacmeister, J. Development of the GEOS-5 atmospheric general circulation model: Evolution from MERRA to MERRA2. *Geosci. Model Dev.* **2015**, *7*, 1339–1356. [CrossRef]
16. Song, Z.; Fu, D.; Zhang, X.; Wu, Y.; Xia, X.; He, J.; Han, X.; Zhang, R.; Che, H. Diurnal and seasonal variability of PM 2.5 and AOD in North China plain: Comparison of MERRA-2 products and ground measurements. *Atmos. Environ.* **2018**, *191*, 70–78. [CrossRef]
17. Randles, C.A.; Sliva, A.; Buchard, V.; Colarco, P.R.; Flynn, C.J. The MERRA-2 Aerosol Reanalysis, 1980 Onward. Part I: System Description and Data Assimilation Evaluation. *J. Clim.* **2017**, *30*, 6823. [CrossRef]
18. Buchard, V.; Randles, C.A.; Da Silva, A.M.; Darmenov, A.; Colarco, P.R.; Govindaraju, R.; Ferrare, R.; Hair, J.; Beyersdorf, A.J.; Ziemba, L.D. The MERRA-2 Aerosol Reanalysis, 1980—Onward, Part II: Evaluation and Case Studies. *J. Clim.* **2017**, *30*, 6851–6872. [CrossRef]
19. Dubovik, O.; Herman, M.; Holdak, A.; Lapyonok, T.; Tanré, D.; Deuzé, J.; Ducos, F.; Sinyuk, A.; Lopatin, A. Statistically optimized inversion algorithm for enhanced retrieval of aerosol properties from spectral multi-angle polarimetric satellite observations. *Atmos. Meas. Tech.* **2011**, *4*, 975–1018. [CrossRef]
20. Dubovik, O.; Lapyonok, T.; Litvinov, P.; Herman, M.; Federspiel, C. GRASP: A versatile algorithm for characterizing the atmosphere. *Spienewsroom* **2014**, *25*, 2–1201408. [CrossRef]
21. Dubovik, O.; Fuertes, D.; Litvinov, P.; Lopatin, A.; Lapyonok, T.; Doubovik, I.; Xu, F.; Ducos, F.; Chen, C.; Torres, B. A Comprehensive Description of Multi-Term LSM for Applying Multiple a Priori Constraints in Problems of Atmospheric Remote Sensing: GRASP Algorithm, Concept, and Applications. *Front. Remote Sens.* **2021**. [CrossRef]

22. Chen, C.; Dubovik, O.; Fuertes, D.; Litvinov, P.; Federspiel, C. Validation of GRASP algorithm product from POLDER/PARASOL data and assessment of multi-angular polarimetry potential for aerosol monitoring. *Earth Syst. Sci. Data* **2020**, *12*, 3573–3620. [CrossRef]
23. Wei, Y.; Li, Z.; Zhang, Y.; Chen, C.; Dubovik, O.; Zhang, Y.; Xu, H.; Li, K.; Chen, J.; Wang, H.; et al. Validation of POLDER GRASP aerosol optical retrieval over China using SONET observations. *J. Quant. Spectrosc. Radiat. Transf.* **2020**, *246*, 106931. [CrossRef]
24. Li, Z.Q.; Xu, H.; Li, K.T.; Li, D.H.; Xie, Y.S.; Li, L.; Zhang, Y.; Gu, X.F.; Zhao, W.; Tian, Q.J. Comprehensive study of optical, physical, chemical and radiative properties of total columnar atmospheric aerosols over China: An overview of Sun-sky radiometer Observation NETwork (SONET) measurements. *Bull. Am. Meteorol. Soc.* **2018**, *99*, 739–755. [CrossRef]
25. Li, Z.; Goloub, P.; Blarel, L.; Yang, B.; Li, K.; Podvin, T.; Li, D.; Xie, Y.; Chen, X.; Gu, X. Method to intercalibrate sunphotometer constants using an integrating sphere as a light source in the laboratory. *Appl. Opt.* **2013**, *52*, 2226–2234. [CrossRef] [PubMed]
26. Li, K.; Li, Z.; Li, D.; Li, W.; Blarel, L. Transfer method to calibrate the normalized radiance for a CE318 Sun/sky radiometer. *Chin. Opt. Lett.* **2015**, *13*, 041001.
27. Ma, Y.; Li, Z.; Li, Z.; Xie, Y.; Fu, Q.; Li, D.; Zhang, Y.; Xu, H.; Li, K. Validation of MODIS Aerosol Optical Depth Retrieval over Mountains in Central China Based on a Sun-Sky Radiometer Site of SONET. *Remote Sens.* **2016**, *8*, 111. [CrossRef]
28. Chin, M.; Ginoux, P.; Kinne, S.; Torres, O.; Holben, B.N. Tropospheric Aerosol Optical Thickness from the GOCART Model and Comparisons with Satellite and Sun Photometer Measurements. *J. Atmos. Sci.* **2002**, *59*, 461–483. [CrossRef]
29. Li, L.; Dubovik, O.; Derimian, Y.; Schuster, G.L.; Lapyonok, T.; Litvinov, P.; Ducos, F.; Fuertes, D.; Chen, C.; Li, Z.; et al. Retrieval of aerosol components directly from satellite and ground-based measurements. *Atmos. Chem. Phys.* **2019**, *19*, 13409–13443. [CrossRef]
30. He, L.; Wang, L.; Li, Z.; Jiang, D.; Sun, L.; Liu, D.; Liu, L.; Yao, R.; Zhou, Z.; Wei, J. VIIRS Environmental Data Record and Deep Blue aerosol products: Validation, comparison, and spatiotemporal variations from 2013 to 2018 in China. *Atmos. Environ.* **2021**, *250*, 118265. [CrossRef]
31. Espinosa, W.R.; Remer, L.A.; Dubovik, O.; Ziemba, L.; Beyersdorf, A.; Orozco, D.; Schuster, G.; Lapyonok, T.; Fuertes, D.; Martins, J.V. Retrievals of aerosol optical and microphysical properties from Imaging Polar Nephelometer scattering measurements. *Atmos. Meas. Tech.* **2017**, *10*, 811–824. [CrossRef]
32. Lopatin, A.; Dubovik, O.; Fuertes, D.; Stenchikov, G.; Parajuli, S. Synergy processing of diverse ground-based remote sensing and in situ data using GRASP algorithm: Applications to radiometer, lidar and radiosonde observations. *Atmos. Meas. Tech.* **2021**, *14*, 2575–2614. [CrossRef]
33. Román, R.; Torres, B.; Fuertes, D.; Cachorro, V.E.; Dubovik, O.; Toledano, C.; Cazorla, A.; Barreto, A.; Bosch, J.L.; Lapyonok, T. Remote sensing of lunar aureole with a sky camera: Adding information in the nocturnal retrieval of aerosol properties with GRASP code. *Remote Sens. Environ.* **2017**, *196*, 238–252. [CrossRef]
34. Hu, Q.; Goloub, P.; Veselovskii, I.; Bravo-Aranda, J.A.; Cheng, C. Long-range-transported Canadian smoke plumes in the lower stratosphere over northern France. *Atmos. Chem. Phys.* **2019**, *19*, 1173–1193. [CrossRef]
35. Zhang, X.; Li, L.; Chen, C.; Chen, X.; Dubovik, O.; Derimian, Y.; Gui, K.; Zheng, Y.; Zhao, H.; Zhang, L.; et al. Validation of the aerosol optical property products derived by the GRASP/Component approach from multi-angular polarimetric observations. *Atmos. Res.* **2021**, *263*, 105802. [CrossRef]
36. Ge, B.; Mei, X.; Li, Z.; Hou, W.; Xie, Y.; Zhang, Y.; Xu, H.; Li, K.; Wei, Y. An improved algorithm for retrieving high resolution fine-mode aerosol based on polarized satellite data: Application and validation for POLDER-3. *Remote Sens. Environ.* **2020**, *247*, 111894. [CrossRef]
37. Li, J.; Wang, G.; Ren, Y.; Wang, J.; Wu, C.; Han, Y.; Zhang, L.; Cheng, C.; Meng, J. Identification of chemical compositions and sources of atmospheric aerosols in Xi'an, inland China during two types of haze events. *Sci. Total Environ.* **2016**, *566–567*, 230–237. [CrossRef]
38. Cao, J.J.; Wu, F.; Chow, J.C.; Lee, S.C.; Li, Y.; Chen, S.W.; An, Z.S.; Fung, K.K.; Watson, J.G.; Zhu, C.S. Characterization and source apportionment of atmospheric organic and elemental carbon during fall and winter of 2003 in Xi'an, China. *Atmos. Chem. Phys.* **2005**, *5*, 3127–3137. [CrossRef]
39. Chen, L.; Wang, Z.; Tao, M.; Wang, X.; Wang, Y. Comparison and evaluation of the MODIS Collection 6 aerosol data in China. *J. Geophys. Res. Atmos.* **2015**, *120*, 6992–7005.
40. Leeuw, G.D.; Sogacheva, L.; Rodriguez, E.; Kourtidis, K.; Georgoulias, A.K.; Alexandri, G.; Amiridis, V.; Proestakis, E.; Marinou, E.; Xue, Y. Two decades of satellite observations of AOD over mainland China using ATSR-2, AATSR and MODIS/Terra: Data set evaluation and large-scale patterns. *Atmos. Chem. Phys.* **2018**, *18*, 1573–1592. [CrossRef]
41. Bond, T.C.; Doherty, S.J.; Fahey, D.W.; Forster, P.M.; Berntsen, T.; DeAngelo, B.J.; Flanner, M.G.; Ghan, S.; Kärcher, B.; Koch, D.; et al. Bounding the role of black carbon in the climate system: A scientific assessment. *J. Geophys. Res. Atmos.* **2013**, *118*, 5380–5552. [CrossRef]
42. Chen, S.; Zhang, X.; Lin, J.; Huang, J.; Zhao, D.; Yuan, T.; Huang, K.; Luo, Y.; Jia, Z.; Zang, Z.; et al. Fugitive Road Dust PM2.5 Emissions and Their Potential Health Impacts. *Environ. Sci. Technol.* **2019**, *53*, 8455–8465. [CrossRef] [PubMed]

43. Li, L.; Che, H.; Derimian, Y.; Dubovik, O.; Zhang, X. Retrievals of fine mode light-absorbing carbonaceous aerosols from POLDER/PARASOL observations over East and South Asia. *Remote Sens. Environ.* **2020**, *247*, 111913. [CrossRef]
44. Wang, L.; Li, Z.; Tian, Q.; Ma, Y.; Zhang, F.; Zhang, Y.; Li, D.; Li, K.; Li, L. Estimate of aerosol absorbing components of black carbon, brown carbon, and dust from ground-based remote sensing data of sun-sky radiometers. *J. Geophys. Res. Atmos.* **2013**, *118*, 6534–6543. [CrossRef]